Summer 2014

Particle Swarm Optimization Using Multiple Neighborhood Connectivity And Winner Take All Activation Applied To Biophysical Models Of Inferior Colliculus Neurons

Brandon S. Coventry
Purdue University

Follow this and additional works at: https://docs.lib.purdue.edu/open_access_theses

Part of the Biomedical Engineering and Bioengineering Commons, Electrical and Computer Engineering Commons, and the Neuroscience and Neurobiology Commons

PURDUE UNIVERSITY
GRADUATE SCHOOL
Thesis/Dissertation Acceptance

This is to certify that the thesis/dissertation prepared

By _Brandon S. Coventry_

Entitled
Particle Swarm Optimization Using Multiple Neighborhood Connectivity and Winner Take All
Activation Applied to Biophysical Models of Inferior Colliculus Neurons

For the degree of ___Master of Science in Electrical and Computer Engineering___

Is approved by the final examining committee:

EDWARD L. BARTLETT, Co-Chair

THOMAS M. TALAVAGE, Co-Chair

MARY L. COMER

To the best of my knowledge and as understood by the student in the *Thesis/Dissertation Agreement. Publication Delay, and Certification/Disclaimer (Graduate School Form 32)*, this thesis/dissertation adheres to the provisions of Purdue University's "Policy on Integrity in Research" and the use of copyrighted material.

EDWARD L. BARTLETT, Co-Chair

Approved by Major Professor(s): _____

Approved by: _M. R. Melloch_   07/22/2014

Head of the Department Graduate Program   Date

PARTICLE SWARM OPTIMIZATION USING MULTIPLE NEIGHBORHOOD

CONNECTIVITY AND WINNER TAKE ALL ACTIVATION APPLIED TO

BIOPHYSICAL MODELS OF INFERIOR COLLICULUS NEURONS

A Thesis

Submitted to the Faculty

of

Purdue University

by

Brandon S. Coventry

In Partial Fulfillment of the

Requirements for the Degree

of

Master of Science in Electrical and Computer Engineering

August 2014

Purdue University

West Lafayette, Indiana

To Jan, Steve, and Chelsea Coventry. Without you, I would have never been blessed with this caliber of an education. Ad majorem Dei glorium

ACKNOWLEDGMENTS

First and foremost, thank you to Dr. Edward Bartlett for his guidance, helpfulness, and patience for this EE whose dreams lie in the field of neuroscience. From my first day in the lab, he has taken exceptional measures to mold me into a god practicing scientist and is always open to my sometimes outlandish ideas. I truly appreciate and look forward to working with him on my doctorate.

I would also like to thank Dr. Tom Talavage for his careful guidance through the bio-aspects of the EE department and keeping me on track with many of the administrative requirements of the department. He has been instrumental in my success here at Purdue and for that, I am eternally grateful. Also, thank you to Dr. Comer for her support and guidance, especially in the field of probability. I am especially grateful for her willingness to discuss ideas within and outside her research field.

I would be remiss not to mention the helpful contributions and general companionship of Aravindakshan Parthasarthy, Emily Han, Jesyin Lai, Ryan Verner, Chris Soverns, Sydney Cason, and all past members of the CAP Lab. I would also like to thank all those here at Purdue who have been instrumental to my success. Especially to Jack Williams, whom I've known since high school and now have the privilege of attending the same institution with him for our graduate work. He has worked tirelessly to make me feel at home and been a constant source of encouragement through academic and life stresses. I must also thank Becky Bercich for her friendship and for guiding me through the ins and outs of the BME department.

TABLE OF CONTENTS

LIST OF TABLES

LIST OF FIGURES

SYMBOLS

A	Amphere
dB	Decibel
S	Siemen
s	Second
V	Volt
Z	Impedance(Ohm)

ABBREVIATIONS

A1   Auditory Cortex

BF   Best Frequency

CIC   Central Nucleus of the Inferior Colliculus

DCN   Dorsal Cochlear Nucleus

DNLL   Dorsal Nucleus of the Lateral Lemniscus

IC   Inferior Colliculus

LSO   Lateral Superior Olive

MGB   Medial Geniculate Body

MSO   Medial Superior Olive

O-U   Ornstein-Uhlenbeck

PSO   Particle Swarm Optimization

Spks/s   Spikes Per Second

VCN   Ventral Cochlear Nucleus

VNLL   Ventral Nucleus of the Lateral Lemniscus

NOMENCLATURE

AMPA α-Amino-3-hydroxy-5-methyl-4-isoxazolepropionic acid

GABA γ-Aminobutyric acid

NADPH   Nicotinamide Adenine Dinucleotide Hydrogen Phosphate Diaphorase

NMDA   N-Methyl-D-aspartic acid

TEA   Tetraethylammonium

ABSTRACT

Coventry, Brandon S. M.S.E.C.E., Purdue University, August 2014. Particle Swarm Optimization Using Multiple Neighborhood Connectivity and Winner Take All Activation Applied to Biophysical Models of Inferior Colliculus Neurons. Major Professors: Edward L. Bartlett and Thomas M. Talavage.

Age-related hearing loss is a prevalent neurological disorder, affecting as many as 63% of adults over the age of 70. The inability to hear and understand speech is a cause of much distress in aged individuals and is becoming a major public health concern as age-related hearing loss has also been correlated with other neurological disorders such as Alzheimers dementia. The Inferior Colliculus (IC) is a major integrative auditory center, receiving excitatory and inhibitory inputs from several brainstem nuclei. This complex balance of excitation and inhibition gives rise to complex neural responses, which are measured in terms of firing rate as a given parameter is varied. A major obstacle in understanding the mechanisms involved in generating normal and aberrant auditory responses is estimating the strength and tuning of excitatory and inhibitory inputs that are integrated to form the output firing of IC neurons.

To better understand IC response generation, biophysically accurate, conductance-based computational models were used to recreate IC frequency tuning responses. The problem of fitting response curves *in vivo* was approached using particle swarm optimization, an optimization paradigm which mimics social networks of flocking birds to solve problems. A new social network modeling winner-take-all activation found in visual neuron coding was developed in which agents are divided into social hierarchies and compete for leadership rights. This social network has shown good performance in benchmark optimization problems and is used to recreate IC frequency tuning re-

sponses which can be used to further understand pathological aging in the auditory system.

1. INTRODUCTION

The ability to hear is central to a person's every day life. It is critical for social interaction, the ability to work, and for personal safety. Due to its integration into every aspect of the individual's daily life, hearing loss is a medical condition that severely affects a patients quality of life. Hearing loss can manifest itself in many ways with several symptoms. First, the ability to hear can be compromised in the peripheral auditory system, including the inner ear, cochlea, and auditory nerve. This damage can occur due to extreme or prolonged noise exposure [1], Ototoxicity [2], or disease [3].Finally, hearing loss can result from developmental changes co-occurring in both the central and peripheral nervous system. Age-related hearing loss (ARHL), also known as Presbycusis, is a prevalent condition whose occurrence roughly doubles from the second to seventh decade of life, affecting 29% of males and 23% of females in their sixties, 39% of males and 37% females in their seventies, and 65% of males and 59% of females in their eighties in the United States [4]. Patients suffering from AHRL often have trouble isolating speech in adverse, noisy listening environments, sometimes known as the cocktail party effect [5,6]. Patients will also often present with side effects of peripheral changes including reductions in the high frequency range and elevated thresholds [7] as well as a loss of processing speed [8]. Along with the reduced ability to hear, patients also experience a variety of other co-morbid psychological symptoms such as feelings of social isolation [9,10], depression [11], and a general reduction in a person's quality of life [10]. Structural MRI studies have linked loss of auditory function with reductions in brain volume [12]. Notably, loss of auditory function can be a marker for Alzheimer's Dementia [13], creating a link of auditory health with normal aging. With its myriad of sensory and psychological symptoms and high prevalence, ARHL is a disease that needs to be treated. Tradi-

tionally, ARHL was thought to be a purely peripheral auditory pathology and has been treated by hearing aids. However, many studies have shown substantial physiological changes throughout the entire central auditory system which are not well treated by traditional hearing aids. To better treat ARHL, central mechanisms of central auditory pathologies must be better understood. To begin, we first conduct a brief review of the auditory system.

As discussed in [14], which will be referred to throughout this discussion, the peripheral and central pathways are complex network beginning with the manifestation of sound as the propagation of pressure waves which first hit the outer ear. The outer ear acts as a filter and a dampening mechanism to ensure effective transduction to middle and inner ear. Within the middle ear, pressure waves reach the tympanic membrane, which converts the pressure wave to mechanical movements through the malleus, incus, and stapes. These ossicles act as mechanical transducers and push against the oval window of the scala vestibuli of the cochlea. Within this fluid filled structure, mechanical energy from the stapes is converted to fluidic energy. The basilar membrane acts as a frequency detector, with a continuum of resonance points along its length which can transduce complex stimuli. This is the first point of tonotopic mapping which will be present throughout the rest of the auditory system. Vibration of the basilar membrane in turn vibrate hair cells on the organ of corti. Movement of these hair cells causes the opening and closing of ion channels at the base of the hair cell stereocilia. This causes changes in neurotransmitter release at the hair cell ribbon synapses that form with auditory nerve fibers. Thus hair cells convert the mechanical motion of the inner hair cells to electrical neural signals which propagate through the auditory nerve. From the auditory nerve, the neural signal is relayed to the auditory brain stem where it first arrives in the central auditory pathway at the cochlear nucleus. The cochlear nucleus then sends projections to the superior olivary complex, trapezoid body, lateral lemniscus, and inferior colliculus [15] and has been

suggested to project to the medial geniculate body in rodents [16].

The inferior colliculus(IC) is a major integrative center, receiving excitatory projections from the dorsal and ventral cochlear nucleus (DCN,VCN) as well as medial and lateral superior olive (MSO,LSO) and inhibitory projections from the dorsal and ventral regions of the lateral lemniscus (DNLL,VNLL), ipsilateral LSO and the superior paraolivary nuclei [17]. The IC also receives feedback projections from layer five of auditory cortex(A1) [18]. The central nucleus of the IC, like the rest of the core auditory pathway, is tonotopically organized. Convergence of inputs from lower auditory structures also create functional zones in the IC with CN and VNLL projections corresponding to monoaural inputs and MSO inputs creating a functional zone for binaural information [19]. The IC contains two functionally distinct cell classes; flat(disc) shaped cells and stellate cells. Within these classes about 20-25% of these neurons are GABAergic with the rest being glutamatergic [20]. The inferior colliculus has its main output projections to the medial geniculate body (MGB) which then projects primarily to auditory cortex. The work presented in this thesis will primarily deal with central nucleus of the IC neuron responses. As such, we continue with an overview of receptive field generation and physiological roles of the IC, which for our purposes only includes the tonotopically organized IC central nucleus, but not the IC dorsal and external cortices.

The concept of the receptive field was first thoroughly explored in the seminal work of Hubel and Weisel [21] mapping the receptive fields of cat visual cortex as well as Barlow mapping receptive fields in frog retinal cells [22]. A cell's receptive field can be thought of as the set of stimulus parameters which can be altered to influence cell responses, such as light intensity and orientation in retinal cells or frequency and level in auditory cells [23]. For example, many studies have shown distinct response classes of IC neurons to sinusoidal tone stimuli, which are but a subset of a continua of frequency response area types [24]. Receptive fields can also be generated from

several types of integration patterns including 1.) inheritance, emerging from inputs with identical functionality, 2.) construction, which is formed by the grouping of functions of the properties of functionally different inputs, and 3.) ensemble, which inherits shared traits from inputs [25]. Receptive field properties can also be studied by using reverse correlation techniques such as spectro-temporal receptive fields, which describes the first order spectral and temporal processing mechanisms of the inferior colliculus [26] and have been used in many studies, including demonstrating that the IC is divided into highly localized spectral and temporal zones [27], the transformation from single to multiple feature selectivity between the IC and A1 [28], and the coding of direction and velocity of frequency modulated sounds in the bat IC [29]. While the MSO is considered the physiological center of binaural tuning, IC neurons also show dual type interaural time differences in slow and fast envelope modulation in sinusoidal amplitude modulated stimuli (SAM) which can be explained by convergent inputs from MSO and LSO [30] while the IC also is implicated in spatial localization via interaural level differences(ILD) which are coding with a balance of excitation and inhibition [31].

One metric of auditory processing in the IC is the frequency tuning curve (FTC). FTCs are elicited from sinusoidal tone stimuli and are used to classify a neuron's best frequency(BF). BFs can be thought of as a neuron's resonance point as it is the frequency at which the neuron fires action potentials at the highest rate. Each neuron in the IC, as it is tonotopically organized, exists in regions with similar best frequencies. A related metric is the neurons response to the sound level of tonal stimuli. Like the neurons BF, there is also a corresponding best level(BL) indicative of the level eliciting the highest spike rate for a particular neuron.

There are several physiological changes in the auditory system that occur due age. First, temporal processing, which is responsible identification of time dependent auditory precepts such as consonants with sharp formant transitions [32] as well as

music [33]. Previous evoked recording studies have shown changes in temporal processing in auditory neural populations due to age in rats [34,35]. Age related changes are also seen in spectral tuning of IC neurons, manifesting in significantly reduced rate-level functions, reduction of frequency selectivity by increased filter widths, and a reduction in "V" shaped frequency response areas [36]. Palombi and Caspary [37] also found a decrease in the number of nonmontonic rate level functions, changes in max firing rates, elevated thresholds and an overall reduction in inhibitory processing in Fischer 344 rat ICs. These changes in summed evoked behavior thus spurs the question of what is physiologically changing to alter these responses. At the level of the IC, Caspary *et al.* have shown decreases in GABAergic markers in aged animals, implying a loss of inhibition [38]. Other studies have also shown increases in parvalbumin, a calcium binding protein, and nitric oxide synthase NADPH correlating to aged auditory brain stem responses and pure tone averages in rhesus monkeys, suggesting a physiological compensation to the decreases in inhibition in the IC [39]. Studies in single unit recordings in the IC show a decrease in the selectivity of the aged neuron along with altered receptive fields compared to young animals, suggesting that offsetting of the excitatory and inhibitory balance gives rise to temporal processing deficits [40].

Knowledge of age related changes in central mechanisms in the auditory pathway has grown substantially. However, exact neural mechanisms of ARHL are still not widely known. Uncovering these mechanisms in biological systems is not a trivial task, as many circuits are difficult to probe. To this end, we utilize computational methods to help elucidate IC central nucleus frequency tuning responses.

2. COMPUTATIONAL METHODS

2.1 Introduction to Computational Neuroscience

Computational neuroscience aims to utilize computational and engineering methods to analyze the nervous system at all levels of abstraction; from the single cell to entire neural networks. Computational neuroscience is primarily driven by the ground breaking work of Hodgkin and Huxely which quantified membrane current recorded from the giant squid neuron both as a network circuit model and as explicit differential equations [41]. Much of the interest in computational methods stems from the fact that, with the advent of more powerful computation systems, complex neuronal dynamics can be easily and rapidly simulated on personal computers. Therefore, a computational model can be used to test a sample stimulus set and make predictions about biophysical outcomes, allowing for a more focused set of stimuli to be used in biological experiments, saving time and resources.

The use of modern computational tools in biology began in the 1960s when molecular biologists began gathering amino acid data sets to assess the information capacity of protein encoding, which was an intractable problem without the aid of computing systems [42]. These tools quickly expanded to neuroscience applications, where analysis of complex systems can be expedited by use of computational systems. Modern computational neuroscience emerged in the 1990s with cellular modeling in visual cortex [43]. In general, computational models fall into two categories; phenomenological and biophysical. Phenomenological models reproduce responses seen in in vivo recordings, but do not model individual ion channel biophysical processes. Biophysical models in general model actual ion channel interactions via numerical analysis

of the Hodgkin-Huxely equations in recreating responses seen *in vivo*. Biophysical models, with the tradeoff of higher numerical complexity, allow for better predictions and more insight into the biological processes that occur. Also, biophysical models can allow for the development of testable hypotheses that can be verified in electrophysiology studies. The choice of each is highly dependent on the level of abstraction and how much the model hopes to explain physiological processes.

Auditory neuroscientists have used computational modeling with great success. Beginning in the periphery, Zhang et al. developed a phenomenological auditory nerve fiber model [44] and extensions [45, 46] of this model have been used in a wide variety of studies, including exploring the role that the medial olivocochlear reflex has on signal in noise detection and discrimination [47], the role speech envelope and temporal fine structure play in speech perception [48], and as inputs in other modeling studies [49]. Like the auditory nerve model, other areas of the auditory pathway have also been modeled, including cochlear nucleus [49, 50], Lateral [51] and medial [52] superior olive, inferior colliculus [53, 54], Medial Geniculate Body [55], and auditory cortex [56]. Computational models are also used to gain insight into physiological mechanisms by probing the system in ways that are difficult or impossible in animal models. Finally, computational models can be integrated into biological experiments. For example, the dynamic clamp, an electrophysiological technique can be used to create a "hybrid computer-biological neural circuits" [57] which allows the model to act as a presynaptic input to a biological process. Here a model neuron can be connected to a biological neuron to probe the biological neuron with novel stimuli which can give deeper insight into biophysical mechanisms. With so many applications and experimental possibilities, computational modeling has become an important component in biological studies. In this work, biophysically accurate conductance-based computational models will be used to recreate physiological responses in order to explore age related changes in frequency tuning in IC neurons. The following sections will discuss model creation and optimization.

2.2 Methods

2.2.1 Single Unit Recordings

Responses were modeled from single unit recordings from young and aged Fischer-344 rats made by another researcher utilizing methods similar to those presented in [53]. In short, single unit recordings were made from the central nucleus of the inferior colliculus(CIC) in a 9' by 9' anechoic sound chamber. Anesthesia was induced by a mixture of ketamine and medetomidine. Anesthesia was reduced for aged animals to account for reduced liver function. Animals were maintained on an oxygen manifold and pulse rate and oxygen saturation were monitored by a pulse-oximeter. A constant body temperature was maintained utilizing a water-circulating heating pad. The IC was located stereotaxically using a rat atlas and physiological recordings, and central nucleus was identified by short latency responses to tones and tonotopic organization.

2.2.2 Computational Methods

For this study, the single compartment conductance based biophysical IC model was adjusted from [53](see Appendix A for model parameters). The model was implemented in NEURON [58] which numerically creates and solves the biophysical ion channel processes. This modeling tool is written in the HOC programming language and individual ion channel models are written in NMODL modeling language. NEURON Models are developed by specifying cell morphology and ion channel types. For this study, lumped single compartment models were used. Overall program control is implemented in MATLAB®, which generates input peri-stimulus time histograms and runs data analysis. The adapting and sustained response models from [53] were adapted in order to model frequency tuning responses. Responses of these models to square pulse current injections can be seen in figure 2.1. The sustained response is based on sustained regular cells seen *in vivo* and are characterized by a large, constant frequency onset and a lower sustained response. The adapting model is based

on the adapting cells seen *in vivo* and are characterized by a high frequency burst followed by lengthening inter-spike intervals with increasing time. The sustained model contains a fast transient Na^+ current (I_{Na}), a delayed rectifier potassium current (I_{kDr}), a high threshold potassium current (I_{kHt}), a TEA-sensitive potassium current (I_{kTEA}), a potassium leak current (I_{leak}), and an Ornstein-Uhlenbeck fluctuating point process current (I_{Gfluct}). The Adapting model includes a fast transient sodium current (I_{Na}), a delayed rectifier potassium current (I_{kDr}), a TEA-sensitive potassium current (I_{kTEA}), low (I_T) and high (I_L) calcium currents, an apamin-sensitive calcium-activated potassium current (I_{Sk}), an apamin-sensitive high conductance calcium dependent sodium channel (I_{Bk}), a hyperpolarization activated cation current (I_h), a potassium leak channel (I_{leak}), and an Ornstein-Uhlenbeck fluctuating point process current(I_{Gfluct}). Kinetics for sustained and adapting models are as follows:

$$\frac{dV}{dt} = \frac{1}{C_{mem}} * (I_{Na} + I_{kDr} + I_{kHt} + I_{kTEA} + I_{leak}) \qquad (2.1)$$

$$\frac{dV}{dt} = \frac{1}{C_{mem}} * (I_{Na} + I_{kDr} + I_T + I_L + I_{kTEA} + I_{Sk} + I_{Bk} + I_h + I_{leak}) \qquad (2.2)$$

While both neurons where available for the model, most results are based on the sustained model. Models were modified to recreate both frequency tuning and level tuning data. In both frequency and level tuning, the user specifies one excitatory and one inhibitory input. Model responses were created assuming inherited receptive fields, but input shapes can be specified for future exploration into receptive field construction. Input nuclei to the IC model were modeled phenomenologically. For the frequency tuning model, Excitatory peri-stimulus time histograms were generated for DCN [59, 60], VCN [61, 62], and LSO [63, 64]. Inhibitory inputs were generated for dorsal [65] and ventral [66] lateral lemniscus.

Input responses were modeled from published recordings phenomenologically as follows. First, based on inputs given by the user, excitatory and inhibitory input peri-stimulus time histograms (PSTHs) are generated. Peri-stimulus time histograms are histograms that represent a summed activity in small bin intervals over a section

of time and can be used to determine the probability of a neuron firing in a certain time interval. To generate PSTH's, input nuclei's best frequency rate, and tuning curve Q10 bandwidth, the bandwidth of the neuron at 10 dB above threshold, were obtained from previous studies. Using this information, the PSTH is generated by declaring a bin size identical to that employed in respective experiments conducted in previous literature. Bins were then created and spikes placed in bin to create a sustained response input corresponding to response statistics. The height of the bins is given by $\frac{k_i}{n*S}$, where k_i is the number of spikes in bin i, n is the number of stimulus repetitions, and S is the bin division. Example PSTHs are shown in figure 2.2. Input
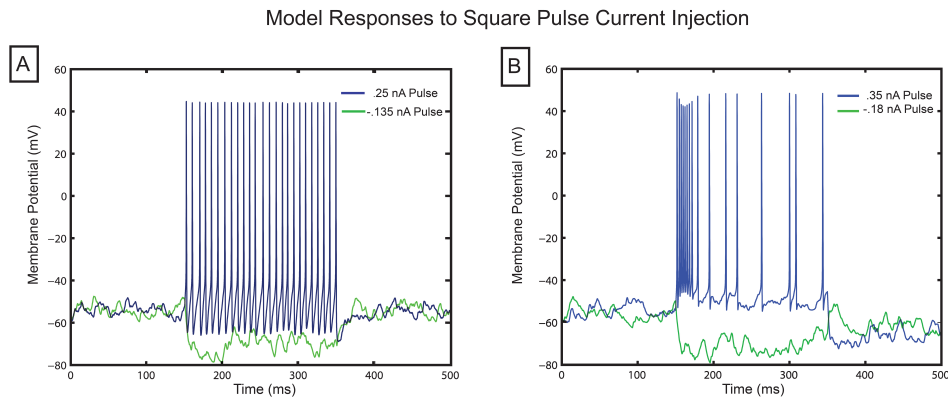
Fig. 2.1. Sustained and Adapting response models to square depolarizing and hyper-polarizing current pulses. A.) Sustained model responses. Sustained firing cells show a near constant frequency spike events under depolarizing currents. B.) Adapting model responses. Adapting cells respond to depolarizing pulses by a onset high frequency burst followed by a responses inter-spike intervals which increase with time

spike times care then drawn according to this distribution. First, a curve is fit to the PSTH to estimate its probability distribution function (PDF) using Matlab's curve fitting toolbox[TM] using Gaussian or Fourier fits(Figure 2.2). The PDF was then integrated to create the cumulative distribution function (CDF). Spike times were then drawn from the CDF using the inverse transform method, which maps a uniform random number to a probability distribution [67], allowing the user to

draw spike times from arbitrary distributions with ease. The inversion method first generates samples of a uniform distribution and then finds

$$X \leftarrow F^{-1}(U) \tag{2.3}$$

where X is now a set of samples, in our case spike times, which are drawn from the input nuclei spike CDF. These spike times are then input into NEURON software. Once in NEURON, excitatory and inhibitory channel kinetics are modeled as in [53].
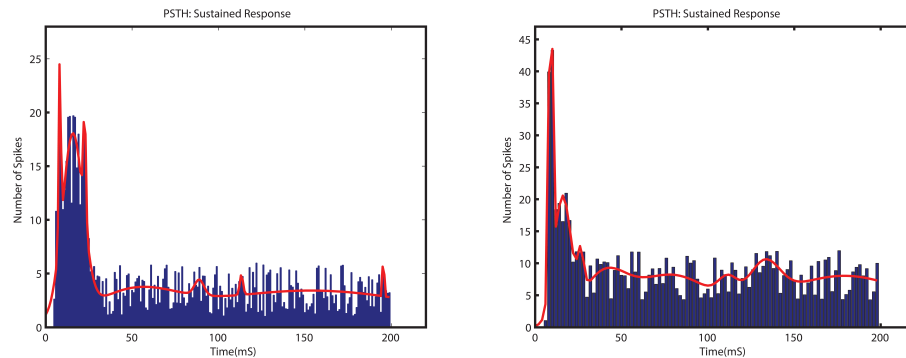
Fig. 2.2. Example input cell PSTHs: Left image displays an example DCN input PSTH and the right an example DNLL input PSTH. In both cases, the red trace shows the fitted PDF

Standard trial runs included 10 repetitions across 64 logarithmicly spaced input tones from .5 to 40kHz. Often, analysis was truncated to an octave around best frequency as outside this area only produces spontaneous activity, and thus carried no additional information concerning the FTC. Tuning curves were generated by calculating mean spike rate per a given stimulus frequency. First spike latency was calculated as the time of the first spike after stimulus onset. Peak latency was measured using a two window method. First, a moderate size window (10ms wide) is generated and sampled across data. In each window, the total number of spikes was calculated. The window with the largest spike rate was selected and subjected to a finer window(5ms) to determine the latency of the peak firing rate, though true IC resolution is much finer than 5ms [68].

Level tuning responses, similar to the frequency tuning model, were created by first modeling input level tuning responses. To replicated results found in *in vivo* recordings, the range of levels modeled was from 4 to 84 dB SPL. In some cases, data for sound levels above 64dB were not available. Rather than extrapolating this data and potentially creating non biological responses, these sound levels were not included. Input rates were modeled from excitatory DCN [59], LSO [63], and VCN [69] inputs, while inhibitory inputs were modeled from DNLL [65] recordings. The model can recreate both monotonic tuning curves, characterized by a sharp increase in firing rate at increasing sound pressure level and saturation of spike rate at BL, and non-monotonic functions, which reach a peak rate and experience a greater than two standard deviation drop in firing rate after reaching BL. Like the frequency tuning model, the level tuning model assumes inherited receptive fields. Figure 2.3 demonstrates model monotonic and nonmonotonic rate level functions. At the start of the model, tone stimuli are assumed to be presented at the neuron's best frequency. Input rate-level functions were modeled phenomenologically. Peri-stimulus time histograms, probability density functions, and input spike times were created as before.

2.2.3 Spontaneous Rate Modeling

A substantial modification to the model in [53] was the addition of spontaneous rate. Spontaneous activity is the observed firing of a neuron without the apparent presence of a stimulus. It is tempting to downplay the significance of spontaneous activity as it is an unevoked response. However, spontaneous fluctuations in neurons raises neuron excitability and even carries information about local network circuits [70], making it a critical component in understanding the neural code. To model spontaneous activity, the membrane potential fluctuations across a neuron need to be modeled. Destexhe *et al.* [71]have previously modeled membrane fluctuations in cortex using an Ornstein-Uhlenbeck noise process. This model was then adapted to
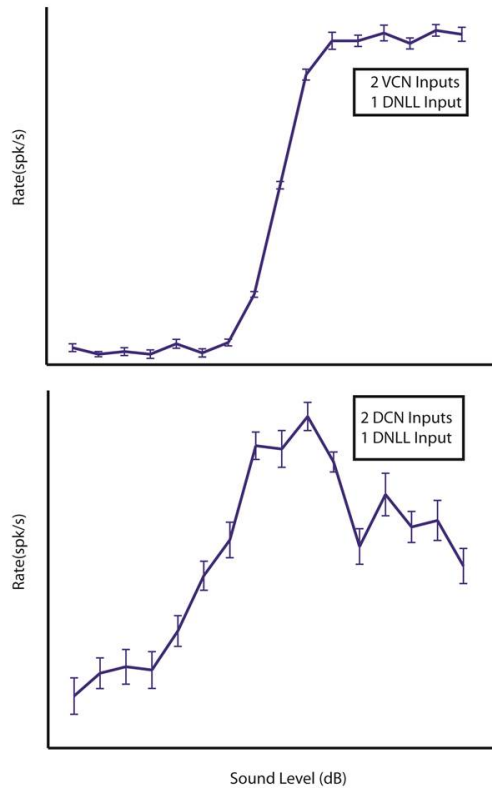
Fig. 2.3. Example of rate-level tuning responses. Top: Monotonic responses. Bottom: Nonmonotonic responses. Responses were classified nonmonotonic if the mean spike rate decreased by 2 standard deviations below the best level.

model spontaneous rates seen in the IC.

The Ornstein-Uhlenbeck (O-U) process is a filtered Gaussian process with a mean reverting characteristic, meaning that given an initial starting condition, the process returns to its mean after a given time. The O-U process for synaptic mechanisms can be reformulated as the following stochastic differential equation [71]:

$$\frac{dg_{e,i}(t)}{dt} = \frac{-1}{\tau_{e,i}}(g_{e,i}(t) - g_{e_0,i_0}) + \sqrt{\frac{2\sigma_{e,i}^2}{\tau_{e,i}}}\xi_{e,i}(t) \tag{2.4}$$

where $g_{e,i}$ designates excitatory or inhibitory conductance respectively, $\tau_{e,i}$ is conductance time constant, σ^2 is the conductance process variance, and $\xi_{e,i}(t)$ is a white

noise process. This process is biophysical in that it has been reformulated to mimic ion channel kinetics. Reversal potentials for excitatory and inhibitory noise processes are $0mV$ and $-75mV$ respectively. Figure 2.4 demonstrates sample O-U excitatory noise paths at varying starting points. The mean reverting characteristic becomes evident in a relatively small amount of time. In this model, the user supplies ex-
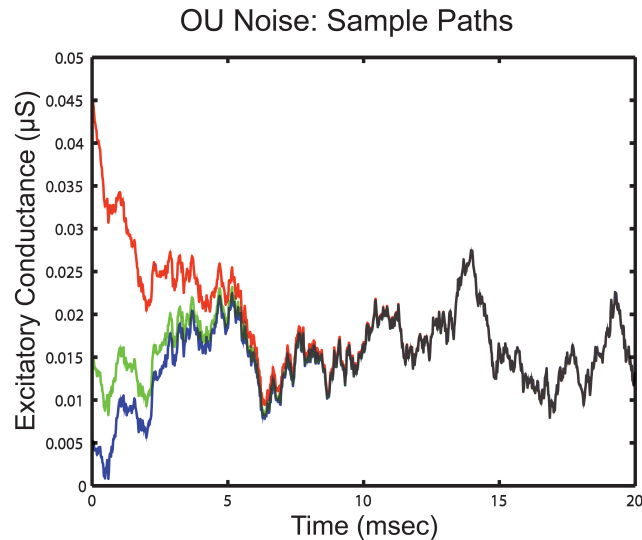
Fig. 2.4. Sample paths of the synaptic O-U process: This figure demonstrates that given 3 different initial starting conditions, after a certain time t the O-U process will eventually return to its mean value. In this figure, the random seeding variable was kept constant to show mean reversion.

citatory and inhibitory conductance mean and standard deviation values as well as respective time constants. While this model was developed for cortical neurons which may have different spontaneous activity in general than subcortical areas, Figure 2.5 demonstrates that this model can be adjusted to model activity seen in the IC, recreating the range mean firing rates and STDs from recorded IC data. With the loss of inhibition due to aging, there is a change in spontaneous activity. This change is subtle: a chi-squared test revealed that there is a higher percentage of aged units with rates greater than 4 Hz ($p < 0.05$)(ASC13 abstract).
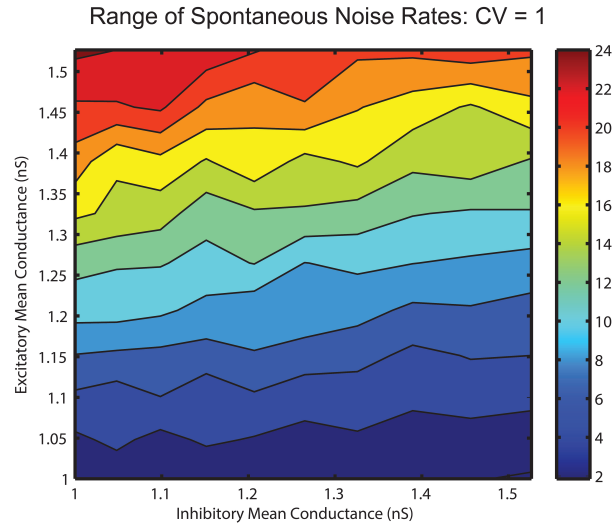
Fig. 2.5. Range of physiologically relevant spontaneous rates recreated in noise model: This figure demonstrates the ability of the OU noise process to recreate spontaneous spike rates seen in young and aged animals. Coefficient of variation for this test was set to 1.

2.2.4 Optimization Using Swarm Intelligence

Optimization procedures provide a fast and robust platform for tuning system parameters to optimize function results or recreate desired responses. Classical optimization procedures, such as linear programming, provide relatively fast and accurate methods for finding optimal solutions for a given problem. However, these methods are ineffective when the problem's derivative is not explicitly known or difficult to approximate. To circumvent this problem, derivative free methods can be employed. The particle swarm optimization (PSO) method was chosen as it can be applied to a variety of general problems, does not require a function derivative, and is relatively simple to implement [72]. Swarm intelligence methods, such as PSO, model flocks of biological organisms, such as swarming bees, colonies of ants, and flocking birds [73], which works on the principle of emergent behavior of groups of simple, individual agents working together in complex social networks to solve problems.

Particle swarm optimization, an evolutionary computational method developed by Kennedy and Eberhart, models the social behavior of flocking birds [72,74]. Problems are formated in the form of fitness functions, which quantify the goodness of fit of the objective. The true power of PSO is embedded in the social networks in which the agents act. The design of social networks is not trivial, as there needs to be a balance between swarming, the movement of agents in a search space, and convergence, the ability for the swarm to come to a solution. Too much emphasis on swarming causes the swarm to loose its objective and diverge, while too much emphasis on convergence will cause the swarm to be trapped in local minima and miss global solutions. To best meet social network and model constraints, a new social structure was developed.

Following the metaphor of flocking birds, each agent is assigned a position and velocity as well as some memory to store its best position. Individually, these agents are simple; it is when these agents are connected in social networks that intelligent problem solving behavior manifests. These social networks are described quantitatively by mathematical graphs (see appendix B). Qualitatively, the social network can be thought of as the instruction set for agent updating and is critical to algorithm performance [75]. The proposed social network bridges the gap between fully informed and canonical ring topologies and can be seen in figure 2.6. At each update cycle, a global leader is decided based on best fitness function value. Then, from each neighborhood, neighborhood leaders are assigned based on agent performance on the fitness function. These leaders act as delegates to the global leader and work to inform neighborhood agents, encouraging them to mimic the leaders actions. The delegates also inform the leader of any better positions found by its constituent members. At first, each member was fully informed, meaning that a neighbor being updated was informed by his fellow neighborhood agents as well as the neighborhood leader. However, this did not provide good solutions and catastrophically failed optimization benchmarks, being significantly outperformed by other social networks. The reason for this failure may lie in the fact that a given agent under update, especially in the

Neighborhood Architecture
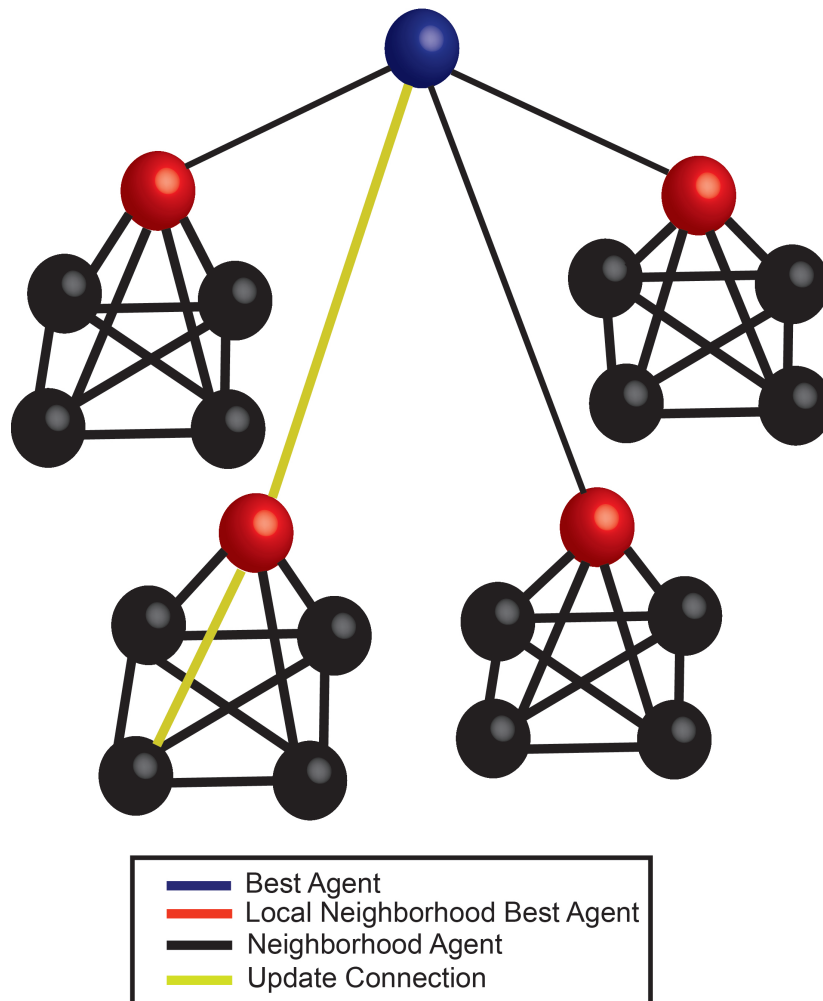
Fig. 2.6. Winner Take All Social Network. Agents are divided into neighborhoods with delegates and a global leader elected by goodness of fitness. Here, agents compete to update other agents, with only good influences able to update agents. This figure demonstrates the update of a delegate. The delegate is updated only by the global leader and the best neighborhood constituent agent.

neighborhoods, is being weighted more by bad influences, agents with poor solutions, than leaders. Therefore, the social network was reconfigured to model the winner take all coding scheme seen in the visual system. In the winner take all (WTA) scheme,

input neurons compete for activation [76, 77], as the target inherits the response of the strongest response of its input neurons while ignoring the rest. In a similar way, agents compete for the ability to update other agents with individual agents only being updated by the agents in its neighborhood with the best fitness. Agents that continually have better fitness are more often allowed to update its neighbors, which may lead to advancement in the social structure. The global leader is only influenced by his past best and the best neighborhood delegate, neighborhood delegates by the global leader and the best constituent, and constituents by the neighborhood delegate and the best neighbor. Update equations are as follows:

$$vbest_{i+1} = \chi * (vbest_i + U(0, \phi_1) \otimes (p_g - xbest_i) + U(0, \phi_2) \otimes (p_n - xbest_i)) \quad (2.5)$$

$$xbest_{i+1} = vbest_{i+1} + x_i \quad (2.6)$$

where χ is the constriction coefficient defined by [74] with $\phi = \phi_1 + \phi_2 > 4$ and

$$\chi = \frac{2}{\phi - 2 + \sqrt{\phi^2 - 4\phi}} \quad (2.7)$$

Typically, $\phi_1 = \phi_2 = 2.05$, leaving $\chi = .7298$ [74]. $U(0, phi_{1,2})$ is a uniform random variable between 0 and $\phi_{1,2}$, p_n is the best delegate position, and $\otimes$ designates a vector multiplication. In similar fashion, delegates are updated according to:

$$vdel_{i+1} = \chi * (vdel_i + U(0, \phi_1) \otimes (p_g - xdel_i) + U(0, \phi_2) \otimes (p_b - xdel_i)) \quad (2.8)$$

$$xdel_{i+1} = vdel_{i+1} + xdel_i \quad (2.9)$$

where p_b is the best neighborhood agent. Finally, individual neighborhood agents are updated according to:

$$vnei_{i+1} = \chi * (vnei_i + U(0, \phi_1) \otimes (p_n - xnei_i) + U(0, \phi_2) \otimes (p_b - xnei_i)) \quad (2.10)$$

$$xnei_{i+1} = vnei_{i+1} + xnei_i \quad (2.11)$$

where p_b is the position of the best neighborhood agent. In general, the PSO algorithm is as follows:

1. Initiate swarm by randomly scattering n agents on solution space
2. Calculate initial fitness values
3. Form neighborhood topology and choose leaders
4. For i iterations:

   Update each agent

   Reassign leadership

   Calculate new Fitness

   end

5. Global best agent is minimum

2.3 Optimization Benchmarks and Sample Problems

Many benchmark problems have been developed to test optimization methods for robustness and error. To test our PSO neighborhood topology, we ran the method on Rosenbrock's function, a common benchmark for Optimization problems. Rosenbrock's function, often called the banana function due to its contour plot, is defined in 2 dimensions as [78]:

$$f(x_1, x_2) = 100 * \left(x_2 - x_1^2\right)^2 + (1 - x_1)^2 \tag{2.12}$$

and in n dimensions as [79]:

$$f(\overline{x}) = \sum_{i=1}^{n} \left[100 \left(x_i^2 - x_{i+1}\right)^2 + \left(x_i - 1\right)^2\right)\right] \tag{2.13}$$

Rosenbrock's function has a global minimum of 0 when $x_1, x_2, ... x_n = 1$. This is used as a protytpe function as it is easy to find local minima, due to the structure of the problem, but much harder to find the global minimum. Figure 2.7 shows the convergence of the PSO method on the 2D Rosenbrock function. In this case, 21 agents were used at 50 iterations. The global solution was found at $x_1 = x_2 = 1$. Collective motions of each agent, shown as blue circles, were tracked and plotted. The fitness function for this optimization was simply the minimum of Rosenbrock's function. Intuitively, higher dimensional problems will be harder to solve. Since our NEURON model is 10 dimensional and computationally costly, we quantify the

Swarm Path: 2D Rosenbrock Function
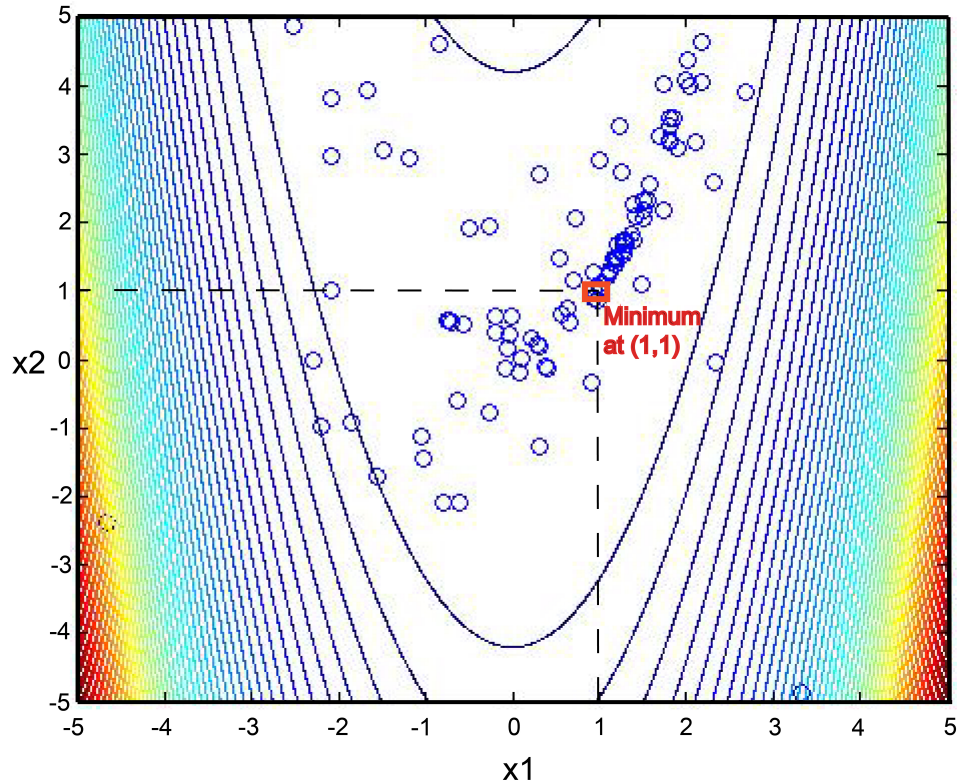
Fig. 2.7. Solution of the Rosenbrock function in 2 dimensions. Individual agent movements were tracked and plotted as blue circles. The program was allowed to run for 50 iterations.

ability of our social network to solve problems at relatively low iterations versus the common ring social network (see appendix B) in similar tests done in Mendes:2004. Optimizations consisting of 1000 swarm updates were completed. Mean and standard deviation values were collected for 500 trials with results are shown in Tables 2.1 and 2.2. As it can be seen, the WTA social network has better mean fitness with smaller deviations in every dimension as compared to the Ring PSO, but not with a different ring update scheme.

When working with stochastic optimization problems, the no free lunch theorem must be considered. The no free lunch (NFL) theorem states that there is no one op-

timization scheme which performs better on all problems than any other optimization scheme. Specifically, when an optimization scheme gains some performance advantage over a set of problems, it looses its efficacy on others [80]. Consider the canonical ring (RingC) network which is topologically the same as the ring network presented earlier, but updates its agents based on the agents best past performance and the best of its two neighbors. Table 2.3 demonstrates the canonical ring performance across Rosenbrock input dimensionality. The addition of updating based on previous experience gives the method a performance advantage on low dimensional problems with a trade off in performance on medium to high dimensional problems. Likewise, WTAPSO trades low dimensional performance for better results in medium to high dimensional problems.

Table 2.1: Performance of WTA social network

Dimension	WTA Mean	WTA STD	WTA Median
2	2.134e-7	1.142e-6	3.606e-9
3	.3823	1.714	3.424e-5
4	1.769	4.6317	0.0293
5	7.1907	36.66	.3595
6	23.966	88.9570	2.437
7	46.0340	121.54	7.81
8	92.76	279.63	16.404
9	182.896	703.4818	25.217
10	229.609	679.226	39.08

Table 2.2: Performance of Ring social network

Dimension	WTA Mean	WTA STD	WTA Median
2	2.134e-7	1.142e-6	3.606e-9
3	.3823	1.714	3.424e-5
4	1.769	4.6317	0.0293
5	7.1907	36.66	.3595
6	23.966	88.9570	2.437
7	46.0340	121.54	7.81
8	92.76	279.63	16.404
9	182.896	703.4818	25.217
10	229.609	679.226	39.08

Another equally important concern with any optimization paradigm is the speed at which solutions are found. Figure 2.8 demonstrates fitness paths of the WTAPSO and Ring PSO. In these tests, the algorithm was allowed to run for 1000 iterations and was repeated 500 times on the 30 dimensional Rosenbrock function (Rosen30). WTAPSO fitness functions decay faster than Ring PSO fitness functions and find better fitness solutions at algorithm termination. In theory this should manifest as better solutions in faster time. To test convergence speed, the Rosen30 function was again used in tests similar to [75]. The algorithm was allowed to run until it reached a fitness value of 10, a very tight fitness for Rosen30 or reached 100000 iterations, indicating a failure of solution convergence. Each optimization was repeated 500 times.

Table 2.3: Performance of RingC Social Network

Dimension	Ring Mean	Ring STD	Ring Median
2	9.861e-35	2.205e-33	0
3	1.146e-9	2.562e-8	0
4	0.918	1.60	3.048e-26
5	3.081	15.593	0.002
6	99.309	569.082	4.021
7	3.484e3	2.651e4	76.356
8	1.424e4	5.092e4	781.860
9	9.290e4	3.130e5	6.402e3
10	2.503e5	6.888e5	4.613e4

As this data suggests, not only does the WTAPSO on average find better solutions, it also finds them much faster. These two traits are critical when optimization problems are high dimensional or has a high cost per iteration. However, one consideration with PSO methods is that it is inherently stochastic, meaning that some starting points and updates may not lead to a convergent solution. This is mitigated by choosing proper model parameters and some intuition on good starting positions. Also, PSO optimization does not guarantee global minimums are found [81]. While this may be critical in some applications, it may not be a concern in cases where solutions are not necessarily unique such as in the reconstruction of neural response curves. However, performance on the convex Rosenbrock function with a global minimum and many local minima is quite good.

Table 2.4: Iteration Run Time

Topology	Mean Iteration	STD	Median
WTA	23070	35066	45375

Swarm Error Path
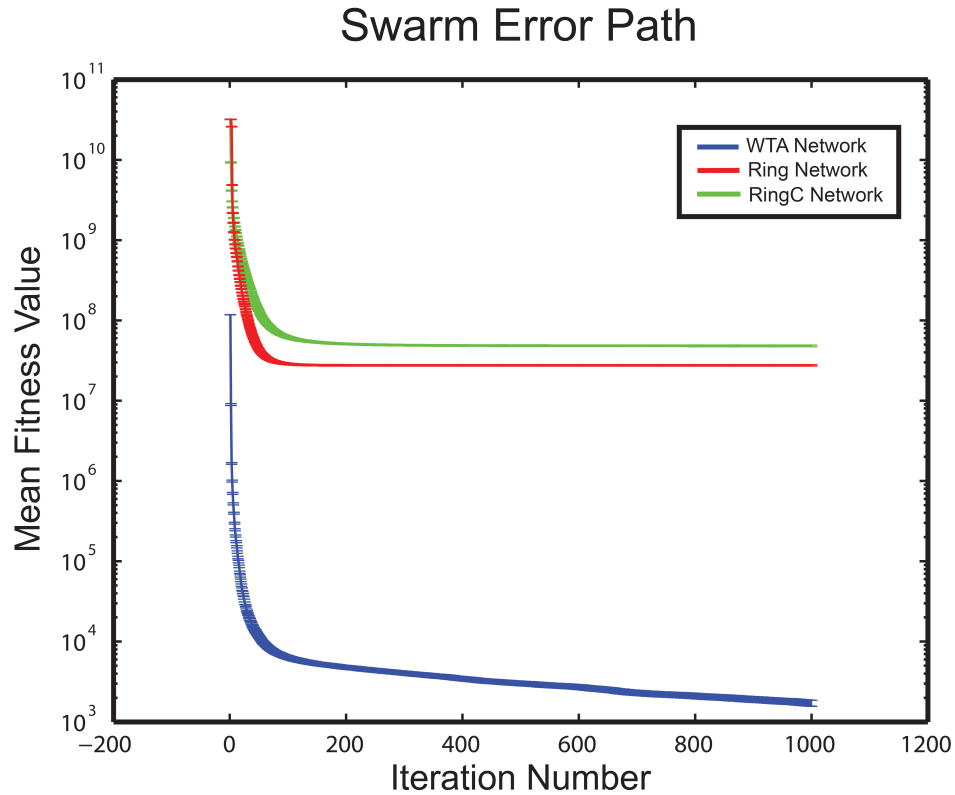
Fig. 2.8. WTA vs. Ring topology run times. Each optimization was allowed to run for 1000 iterations and was repeated 500 times. WTAPSO shows much sharper slopes and overall better fitness than Ring topologies over the 30 dimensional Rosenbrock Problem at algorithm termination.

The same test was applied to the ring topology. After an extended run time, only 70 iterations could complete with 0 optimizations reaching tolerance. It should be noted that a tolerance fitness value of 10 is much tighter than what is seen in [75]. More telling is that our method was able to meet this fitness well within 100000 iterations while the ring could not. When applied to biological optimization problems, such good performance on high dimensional test problems should translate to better solutions in a lower iteration time than traditional or canonical particle swarm methods.

3. RESULTS

Computational models can be used to make predictions about neural responses and elucidate mechanisms involved in response generation. In this section we will explore how well the proposed model recreates IC frequency tuning neuron responses.

3.1 Spontaneous Rate Modeling

Spontaneous spiking activity resulting from membrane voltage fluctuations is an important component in the modeling of response generation processes. To test the effects of hyper-excitability due to spontaneous rates, model responses were created in the presence of mean spontaneous rates seen *in vivo* in young and aged rats (Table A.3.) and compared to noiseless responses. To quantify difference, a percent difference metric was used. Figure 3.1 demonstrates the effect synaptic fluctuations and spontaneous rate have on frequency tuning curve responses in young animals. While it is expected that there is a large increase in zero response regions where spontaneous rate dominates the response, there is also a large change within the tuning curve including as much as a 20 percent difference around BF. This supports the observation that synaptic noise increases excitability leading to higher firing rates than would be seen in relatively silent recordings such as *in vitro* slice recordings. This effect was also be studied in aged responses, as shown in Figure 3.2, demonstrating that aged responses increase in firing rate compared to young responses (20 vs 40 percent difference) as well as a shift in the position of BF. These changes in frequency tuning response properties in the presence of O-U noise give credence to spontaneous activity's role in raising membrane excitability and will be used for the remainder of the computational experiments. These two figures are used to illustrate changes that

may occur in the presence of spontaneous activity, but individual features such as shifts in BF may not be general due to the stochastic nature of the input.

Effect of Spont Rate on FTCs: Young
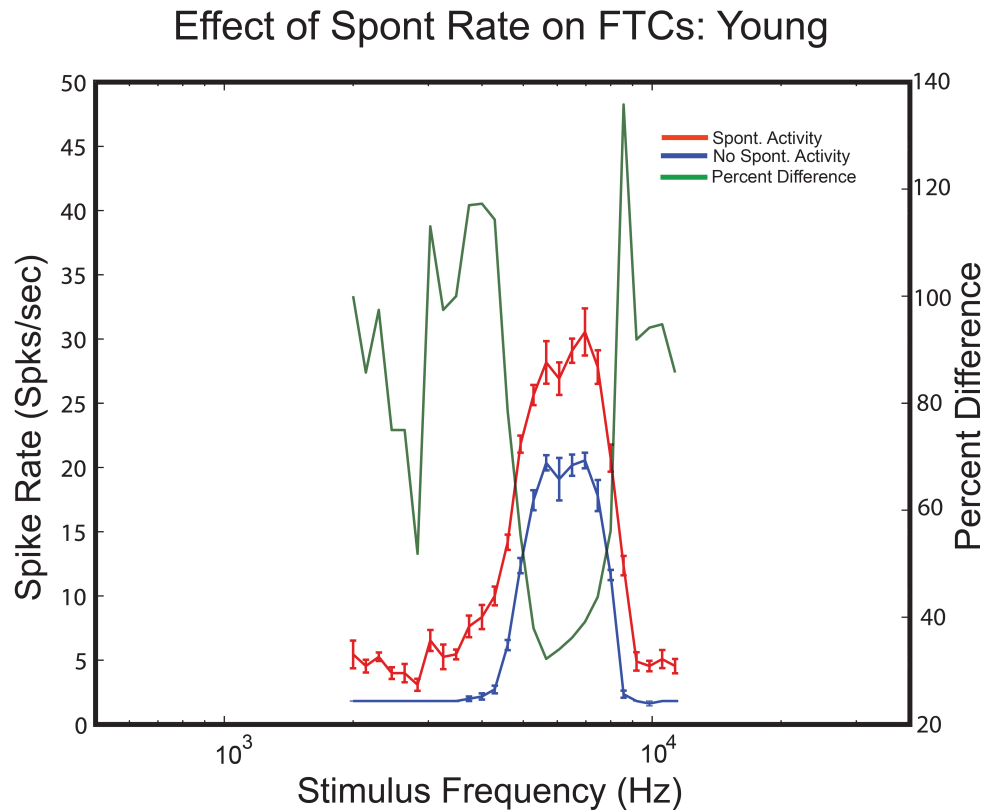
Fig. 3.1. The effect of spontaneous activity on frequency tuning curves is large, creating a nearly 20 percent increase in responses at BF. The blue trace corresponds to the noiseless model, the red to the model with spontaneous activity, and the green line to the percent difference.

3.2   Frequency Tuning

The IC is a tonotopically organized nucleus with spatial distribution of best frequencies. *In vivo* responses were elicited from tone stimuli as described earlier. First, mean spontaneous rates were fixed. For a young animal model, experimentally found excitatory noise conductance value of 0.935 nS and inhibitory conductance value of 0.5nS were used to set a mean rate of 2.449 spikes per second, similar to what has

Effect of Spont. Rate on FTCs: Aged
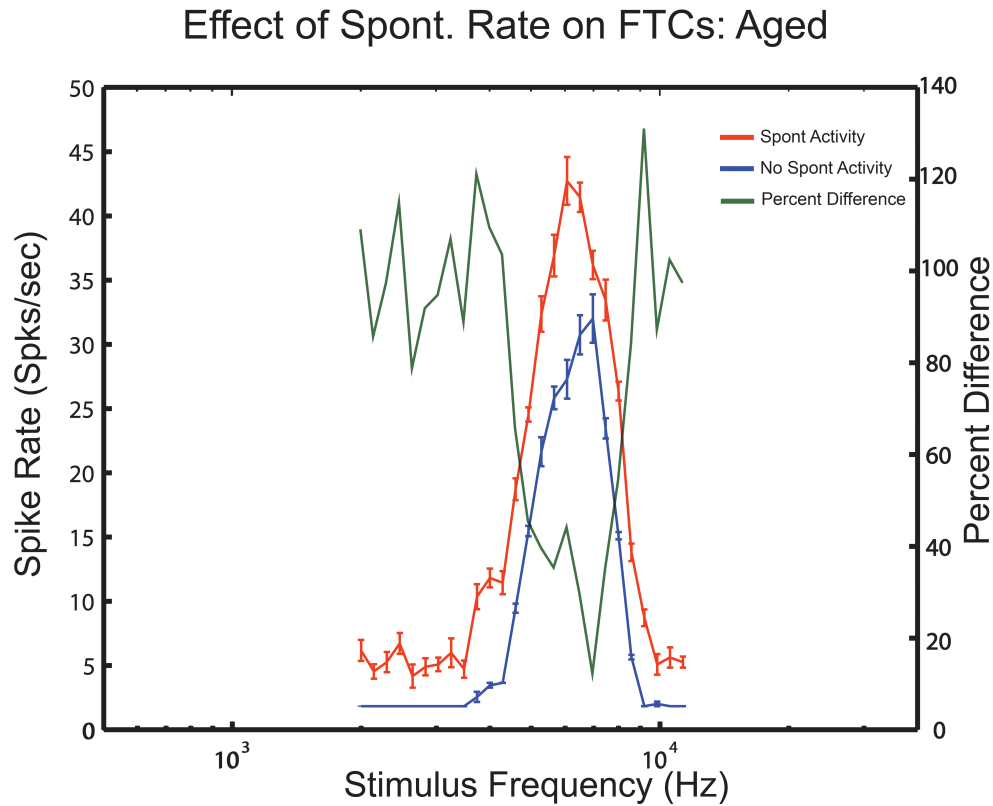
Fig. 3.2. Like young neurons, the effect of spontaneous activity on frequency tuning curves is large in aged neurons. In this case, the presence of *in vivo* like noise shifts the location of the BF under identical inputs.

been recorded in our studies. To recreate an aged response, inhibitory conductance was lowered to 0.29nS, which generated a firing rate of 3.42 spikes per second which is again similar to what has been seen in our lab(for full details on input parameters, see Appendix 1). Figure 3.3 shows an example of a recreated neuron from a young rat with a BF of 6.5kHz. In this model, inputs into the IC cell were 3 LSO and 3 DNLL inputs with AMPA and NMDA conductances set to 100 percent and GABA set to

75 percent. Goodness of fit, characterized by a mean square error metric, was 276.3. To recreate aged responses, GABAa conductance was lowered, reflecting the loss of

Recreation of FTCs: Young Neuron
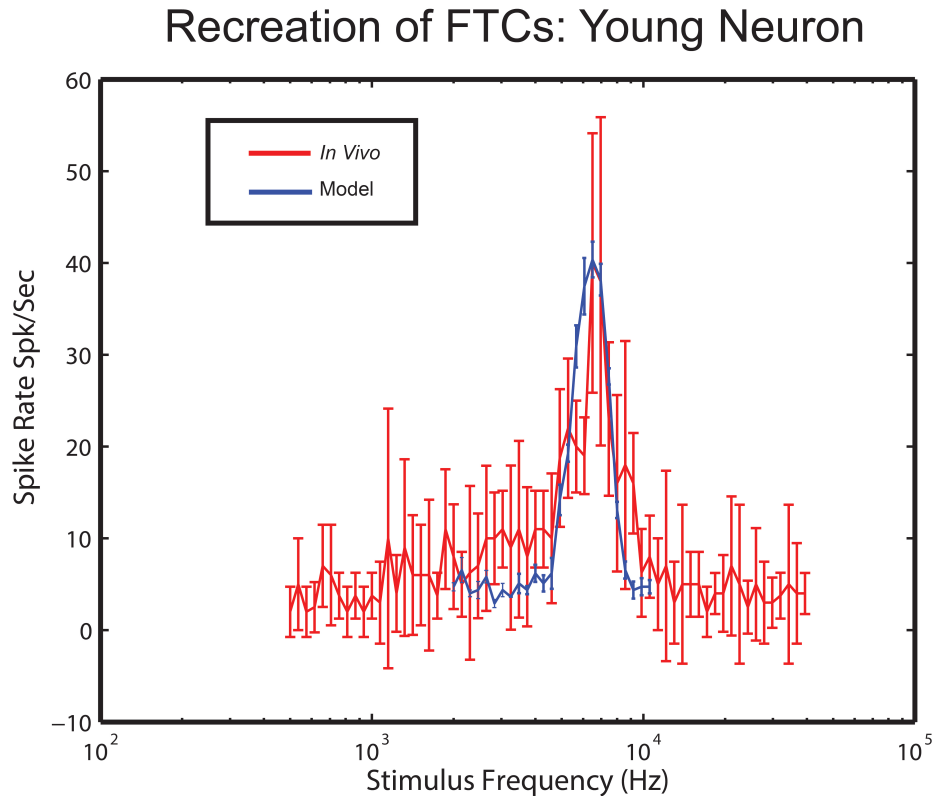
Fig. 3.3. Recreation of a young frequency tuning curve. Model inputs were 3 LSO and 3 DNLL inputs. AMPA and NMDA strength were set to 100 percent while GABAa conductance was set to 75 percent. Mean square error was 276.3

GABA-ergic markers seen in aged rats as discussed earlier. Figure 3.4 demonstrates the recreated aged responses. To better understand the mechanistic changes in aging and to reduce the confounding effects such as tuning curve width changes in shifted BFs, an aged neuron at the same BF as Figure 3.3 was used. AMPA and NMDA strengths were kept constant, but GABAa conductance strength was lowered 35% from the young model. Mean square error for this reconstruction was 230.8. For each model, spontaneous rates were set to recreate mean values seen in young and aged neurons respectively. While aged response shape were recreated by simply lowering
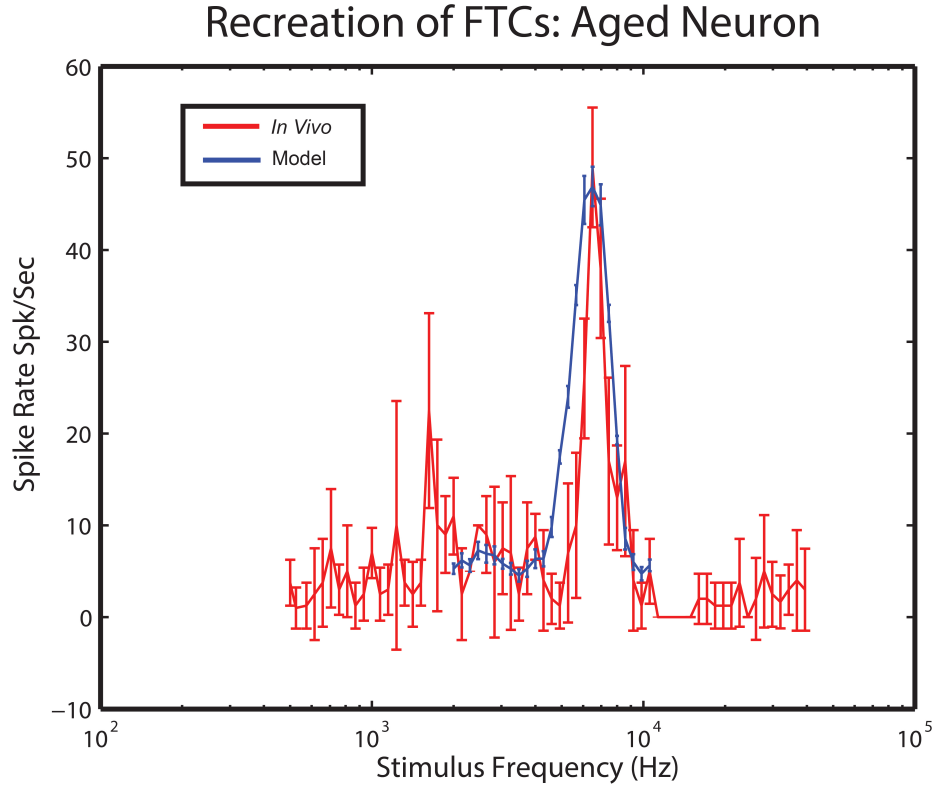
Fig. 3.4. Recreation of an aged frequency tuning curve. Model inputs were 3 LSO and 3 DNLL inputs. AMPA and NMDA strength were set to 100 percent while GABAa conductance was set to 40 percent. Mean sqaure error was 230.8

inhibition, actual auditory neural changes leading to central auditory deficits are certainly more complex. For example, compensation mechanisms may work to correct inhibition decreases [37]. Other variables, such as inhibitory latency and input time constants may also change. With the multiplicity of variables active in the system, fitting responses by hand precisely becomes far to difficult. Therefore, the particle swarm optimization paradigm will be utilized to logically fine tune input variables to recreate IC responses.

3.3 Level Tuning

Level tuning characterizes a neurons response to pure tones at varying stimulus presentation levels. As demonstrated earlier, the computational model can create two classes of responses, monotonic and nonmonotonic(Figure 2.3). To test the ability of the model to recreate level tuning responses, the model was fit by hand using *in vivo* data. Figure 3.5 demonstrates a recreated nonmonotonic response. Error was calculated as the mean sqaure error of model and *in vivo*. Spontaneous rates were set as a young response. Model response is truncated after 64 dB due to unavailable data.
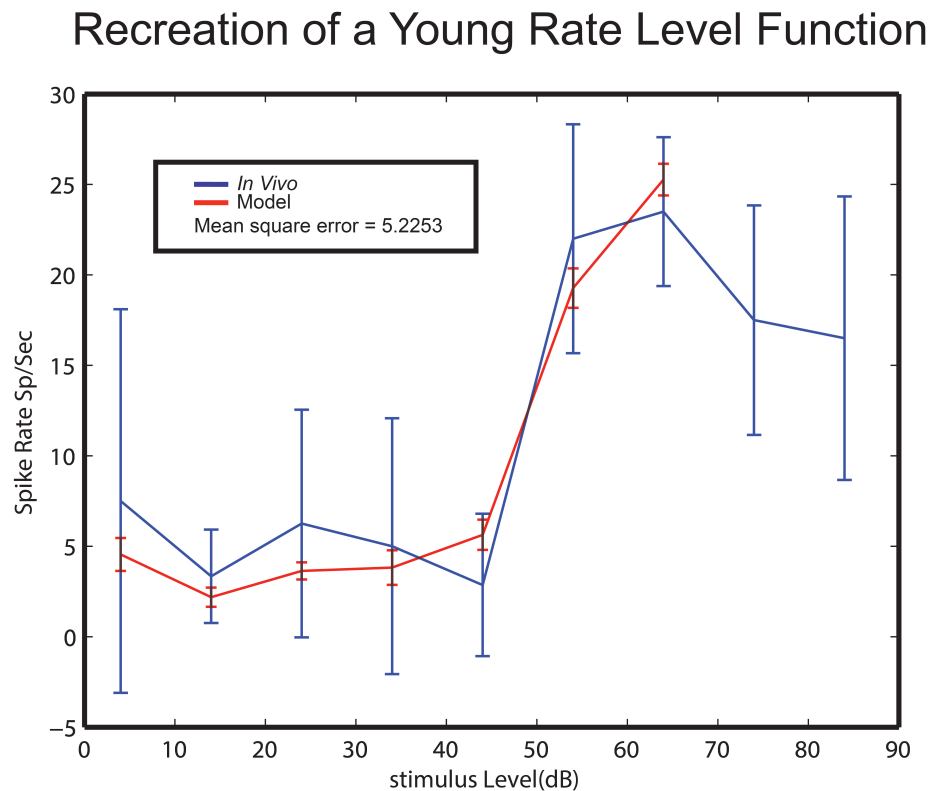

Fig. 3.5. Recreation of a level tuning neuron response. Inputs were 2 LSO and 1 DNLL with AMPA and NMDA set ot 27 percent and GABAa set to 30 percent. Mean square error = 5.2253

3.4   Response Recreation using Particle Swarm Optimization

The ability to recreate IC responses from *in vivo* recording would allow for valuable insight into neural response creation. To this end, the winner take all particle swarm optimization method was utilized. The model was adjusted such that only 1 AMPA, 1 NMDA, and 1 GABA input were used, and allowed its conductance strength to vary. The lumping of these parameters is a reasonable simplification and allows for a dimensionality reduction in optimization. Input parameters optimized over were AMPA, NMDA, and GABA conductance values and time constants and inhibitory input delay, creating an optimization over ten variables. For our fitness function, it is important to recreate not only response magnitude, but to preserve response shape as well. Therefore, we utilized a fitness function that has been used in x-ray reflectivity to fit data that consists of highly oscillatory data [82]. The function is as follows:

$$F = 1 - \left(1 + \left[RMSE(x_c, x_m)\left[1 + r(x_c, x_m)\right]\right]^{-3}\right)^{-1} \tag{3.1}$$

where x_c is the calculated, model curve, x_m is the recorded curve, $RMSE$ is the root mean square error function, and r is the correlation coefficient between x_c and x_m. For this function, lower fitness values correspond to better fits. Tuning curves were generated at ± 1.5 octaves around BF. This captures the entirety of the tuning curve plus some of the spontaneous activity at the tails. The rest was truncated as it would only generate spontaneous activity. While *in vivo* response curves were created with ten repetitions of the stimulus, this caused an unacceptable run time for the swarm method. Since most IC responses modeled were well driven, a compromise of 5 repetitions of each stimulus was used. Figure 3.6 demonstrates the reconstruction of a young neuron tuning curve after 50 iterations. While the recreated response has a faster firing rate at BF, the difference is small (4.3672 spks/sec) and within one standard deviation of the recorded response. The shape has been well reconstructed with a 50% firing rate bandwidth differences between model and recorded responses of 396 Hz.

Table 3.1: Young Reconstruction

Parameter	Value
AMPA %	205.3723
NMDA %	226.9570
GABA %	124.3821
AMPA τ_1(ms)	1.0963
AMPA τ_2(ms)	5.8759
NMDA τ_1(ms)	32.1961
NMDA τ_2(ms)	50.4178
GABA τ_1(ms)	2.8390
GABA τ_2(ms)	14.9868
GABA delay(ms)	1.1908

Next, an aged neuron was reconstructed. Earlier reconstructions have simply lowered the inhibition strength while keeping excitation and other parameters set. While this is a decent approximation, certainly other parameters change with age, owing to compensation mechanisms, membrane property compensation, or age related changes. Therefore, the swarm was reinitialized and allowed to run on the aged response. Figure 3.7 demonstrates the recreation of an aged neuron utilizing LSO excitatory and DNLL inhibitory inputs.

Table 3.2: Aged Reconstruction

Parameter	Value
AMPA %	199.5712
NMDA %	109.4907
GABA %	61.7082
AMPA τ_1(ms)	0.2080
AMPA τ_2(ms)	6
NMDA τ_1(ms)	32.9026
NMDA τ_2(ms)	51.5274
GABA τ_1(ms)	2.8959
GABA τ_2(ms)	15.3124
GABA delay(ms)	-2.7914

Light bounds were placed on neurotransmitter conductance strengths to prevent variables from reaching nonphysiological negative values. Spontaneous rate was set to match what was seen in *in vivo* recordings and optimized parameters are reported in Table 3.2. Again responses were well recreated with a peak spike rate difference of 6.0865 spks/sec, a 50% bandwidth difference of 536 Hz, and fitness of 0.3649.
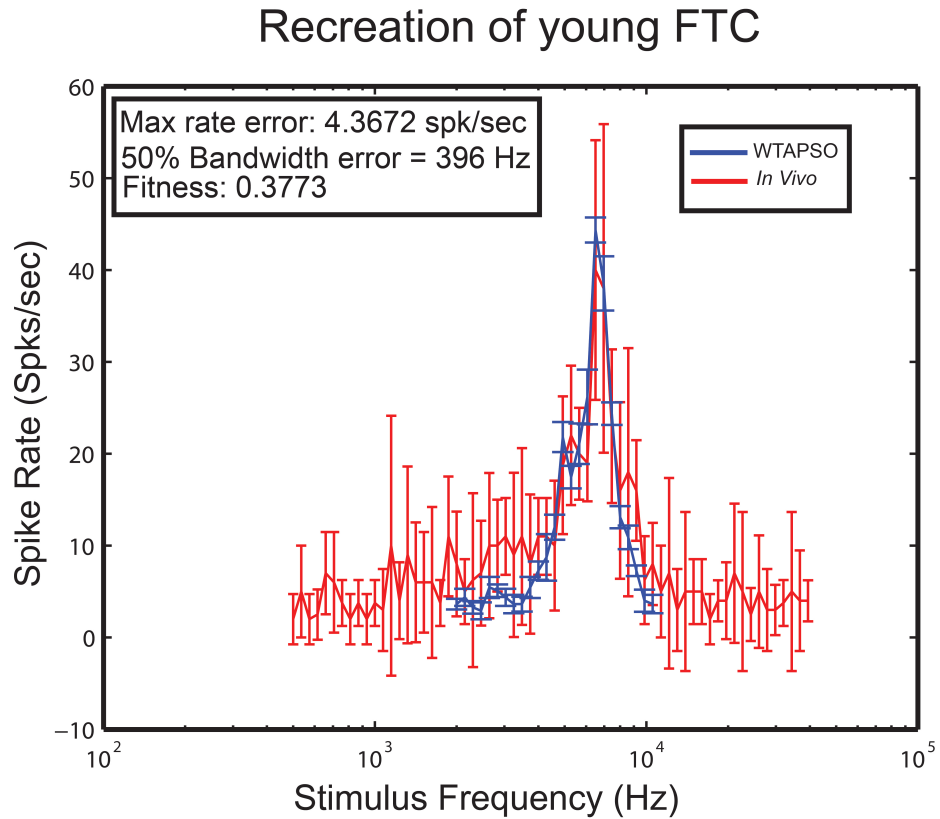
Fig. 3.6. Recreation of a young neuron tuning curve. Fitness for this graph was .3773 after 50 iterations
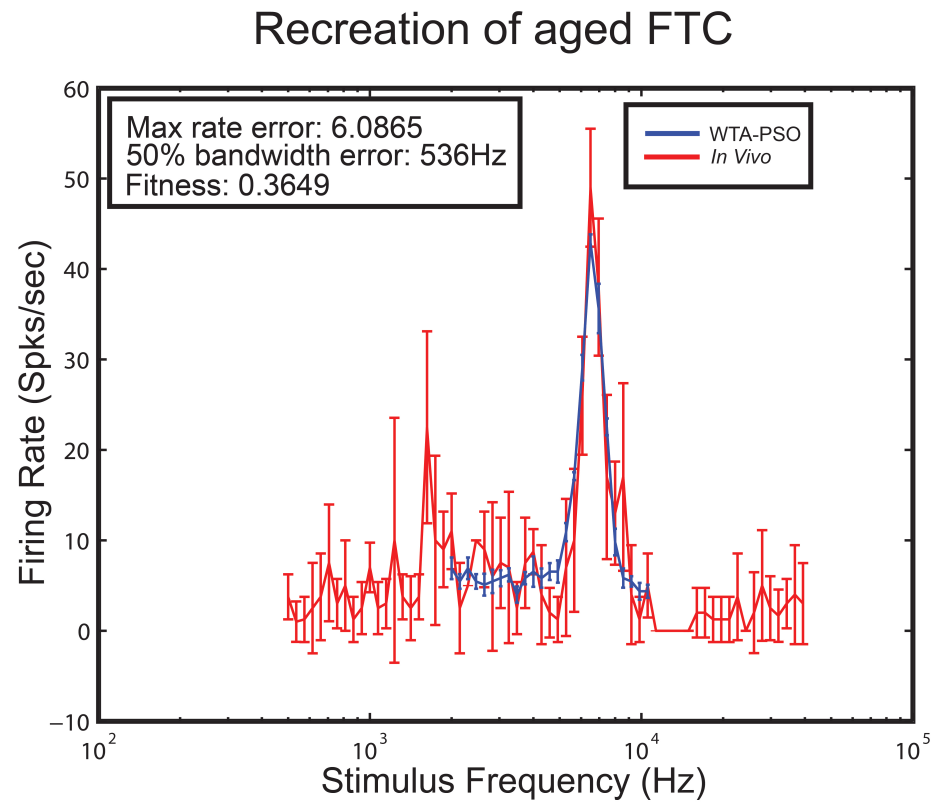
Fig. 3.7. Reconstruction of an aged neuron response. Optimization routine was identical to that of the young response. Fitness criterion for this response was 0.3649 after 50 iterations

4. DISCUSSION

4.1 Computational Models

In this study, neuron spontaneous activity, frequency tuning, and level tuning were modeled and fit to experimental data. In the spontaneous rate case, our results demonstrate the importance of modeling spontaneous activity. Physiologically, membrane voltage fluctuations may come from the flickering of ion channels and contains information that can describe overall network architecture [70]. Our model results show that spontaneous activity has a nontrivial impact on membrane excitabilty and, given identical stimulus parameters, may increase firing rate by 20 to 30 percent. This can be further tested in slice recording experiments by use of dynamic clamp techniques. Our results also extend Rudolph and Destexhe's O-U noise model [71] to mid brain IC neurons and can recreate spontaneous rates seen in young and aged rats.

Utilizing and extending the IC model presented in [53], we were able to recreate frequency tuning curves seen in young and aged rats. While tuning curves are fairly recreated with a young mean square error of 276.3 and aged mean square error of 230.8. Error in the aged model can possibly be explained by the fact that this study was cross sectional and from a different animal. While the young response did have a narrower tuning width(Q50 $\approx$ 1402 Hz) as compared to the aged neuron(Q50 $\approx$ 2722 Hz) as expected, the model results by simply lowering inhibition recreates an aged response with a much wider bandwidth. This is most likely caused by the fact that the model assumes co-tuned inhibition as opposed to lateral inhibition. Rerunning the model with lateral inhibition on the falling edge changed the response shape (Figure 4.1) with a slight increase of mean square error (231.0449). Tuning width also seems

to be a function of input driving strength as well, with higher input conductances giving rise to wider tuning curves(Figure 4.2) for certain input conditions. Eventually, lateral inhibition will be included in the PSO optimization variables. It should be

Lateral Inhibition: Aged Response
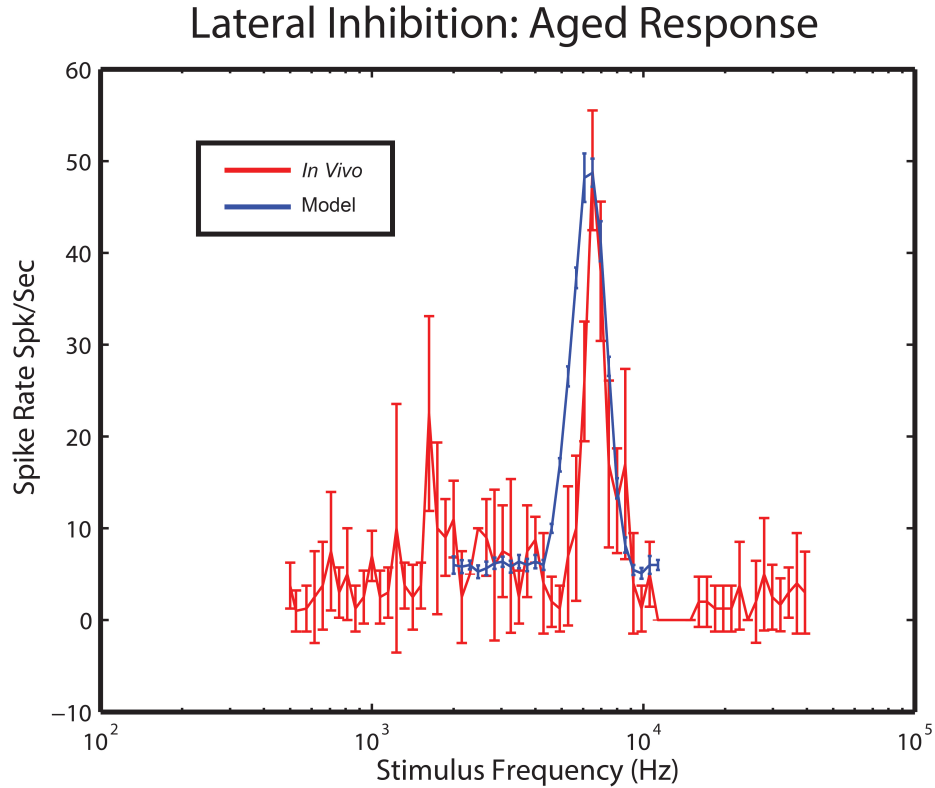
Fig. 4.1. This model utilizes lateral inhibition at 6964Hz to decrease bandwidth. Mean square error = 231.0449. This demonstrates that modulation of inhibitory BF of the FTC can alter tuning curve widths in our model.

also noted that these results are not unique in the sense that there is a one-to-one mapping of input parameters to response type. This can be easily mitigated by swarm optimization by allowing the best frequency of the inhibitory input to vary slightly about a point.
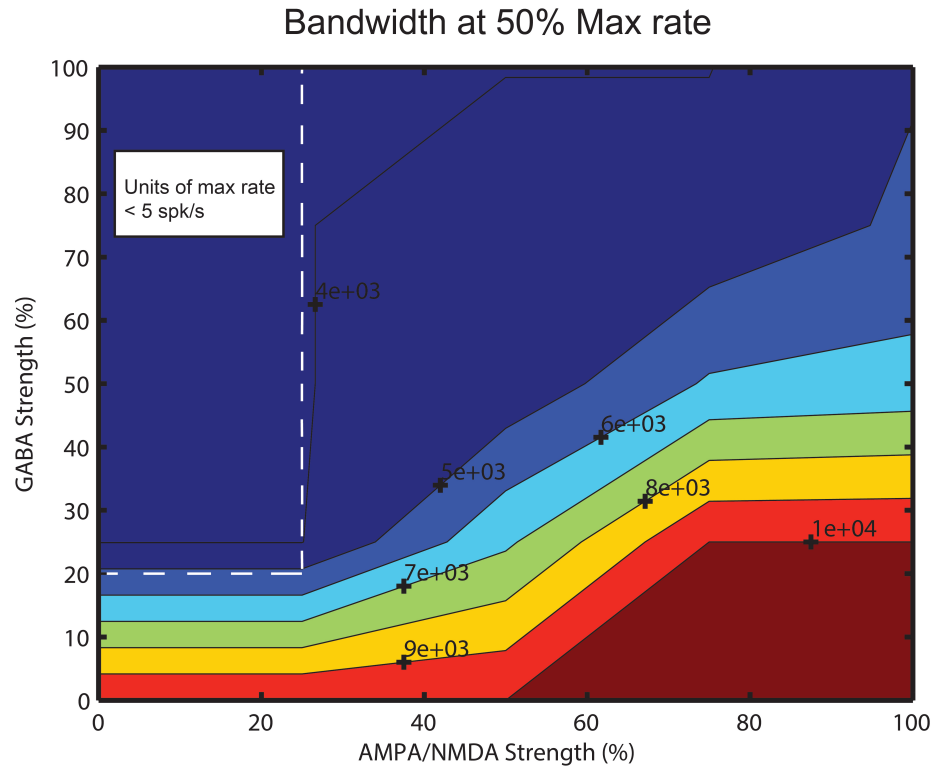
Fig. 4.2. The effect of conductance strength on tuning bandwidth is seen here. It is seen that at higher excitatory conductances that tuning curves tend to widen in the model

4.2 PSO response recreation

Frequency tuning response curves were reconstructed autonomously utilizing a new particle swarm optimization network that models winner-take-all coding schemes seen in the visual system. While results had good fitness values, there is room for improvement. The primary source of error stems from the fact that excitatory and inhibitory inputs were individually aggregated. Additional inputs from other input nuclei should further shape tuning curves, including implementing lateral inhibition into age models to attempt to explain bandwidth changes in aged responses.

A key aspect of neuron response recreation via particle swarm optimization is whether or not optimized results are physiologically relevant. In some cases, WTAPSO

was allowed to run unconstrained with no physiologically adverse results. However, some input sets resulted in neurotransmitter conductance values which were negative. The resulting fits, however, were quite good, as can be seen in Figure 4.2. Particle swarm optimization is a purely unconstrained optimization paradigm owing to its derivative free nature [83]. Therefore, any constrained optimization must be converted to an unconstrained problem which can be done via a variety of techniques [84]. However, Poli *et al.* [74] suggest that light constraints that bound maximum or minimum values of an agents position are acceptable with unconstrained PSO. Results shown in Figure 4.2 demonstrate the necessity to evaluate model results for physiological relevance. However, as demonstrated earlier, light bounds do seem to allow for physiologically relevant input parameters.

Finally, in non-optimized reconstructions, aged responses were constructed from young responses by simply lowering the inhibitory conductance value. In recreating the aging mechanism, it is expected to see a similar decrease between young and aged reconstructions utilizing the same inputs. Figure 4.3. displays the recreation of a young neuron response curve using LSO and DNLL inputs. The optimized results will be compared the aged response recreation in Figure 3.7. Transitioning between the two resulted in a 43% change in GABA conductance strength, on order with what was done in non-optimized reconstruction. AMPA conductance strength changed only slightly with a percent change of -15%. NMDA conductance, however, had a fairly drastic change of 97%. This may not completely reflect physiology and may lessen the effect of decreased inhibition. Future tests will explore this mechanism by reformulating the optimization problem to more tightly constrain excitatory conductance values.
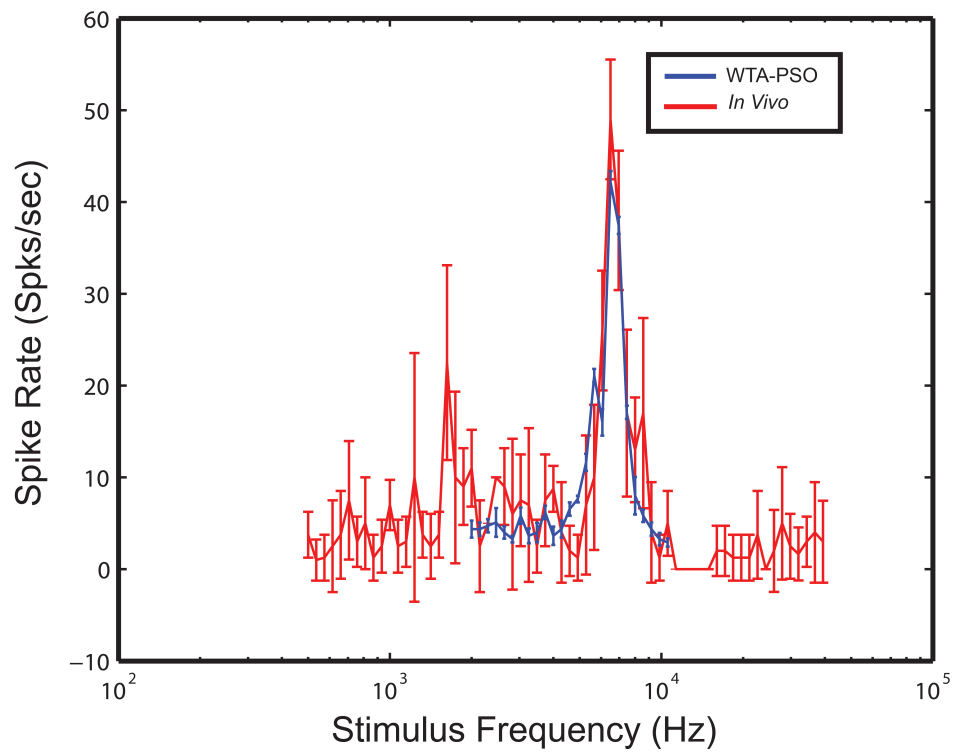
Fig. 4.3. Some input sets can recreate neuron frequency tuning curves quite well, but do so with negative neurotransmitter conductance values. This curve had a fitness function value of 0.4313.

5. FUTURE WORK

5.1 Further Improvements to WTAPSO

Inducing competition into PSO comes with the tradeoff that many more agents are lost, meaning that they no longer make progress towards better solutions. While performance using this method is better in medium to high dimensions as compared to ring topologies, these lost agents constitute an unnecessary computational load. The next version of this method will include a grim reaper scheme, in which agents who do not make effective progress are reinitialized and placed back into the neighborhood. In theory, this will kick out the agent from local minima that has trapped it. It will introduce more competition into the system as well, as more agents will be viable update candidates and should improve algorithm performance further with only slightly higher computational load.

To further improve performance, multi-pass optimization will be utilized. Input parameters will be optimized as discussed in this work. Once these parameters are found, they will be fixed and more excitatory and inhibitory inputs will be placed into the cell. This mimics the convergence on many inputs into the IC and should also allow for better response fitting as well. Finally, the WTAPSO will be extended to a multi-objective paradigm. This will allow for more complex modeling of individual neuron parameters, such as competing spontaneous rate parameters. As a major source of error, optimizing input spontaneous rate, which is a function of 4 dependent parameters, will better recreate responses and drive fitness error down.

5.2 Multicompartment and network modeling

Our current model consists of a single compartment containing all ion channels and point processes. While this is a good approximation to an IC neuron, several biophysical processes, such as dendritic processing, a missed. By creating a more realistic representation of IC neuron geometry, better predictions can be made with regards to relevant biophysical processes.

Another aspect that the neuron model currently does not account for is the fact that IC neurons receive feedback projection from interneurons within the IC as well as projections from layer V of auditory cortex [18]. This network architecture can account for more complex forms of inhibition as opposed to simple co-tuning or lateral inhibition in the current model and can thus be used to recreate complex responses.

LIST OF REFERENCES

LIST OF REFERENCES

[1] M. Basner, W. Babisch, A. Davis, M. Brink, C. Clark, S. Janssen, and S. Stansfeld, "Auditory and non-auditory effects of noise on health," *The Lancet*, vol. 383, no. 9925, pp. 1325–1332, 2014.

[2] J. Schacht, A. E. Talaska, and L. P. Rybak, "Cisplatin and aminoglycoside antibiotics: Hearing loss and its prevention," *The Anatomical Record*, vol. 295, no. 11, pp. 1837–1850, 2012.

[3] G. Rance, M. M. Ryan, K. Bayliss, K. Gill, C. O'Sullivan, and M. Whitechurch, "Auditory function in children with charcot-marie-tooth disease," *Brain*, vol. 135, pp. 1412–1422, 2012.

[4] T. Yamasoba, F. R. Lin, S. Someya, A. Kashio, T. Sakamoto, and K. Kondo, "Current concepts in age-related hearing loss: Epidemiology and mechanistic pathways," *Hearing Research*, vol. 303, pp. 30–38, 2013.

[5] E. M. Z. Golumbic, D. Poeppel, and C. E. Schroeder, "Temporal context in speech processing and attentional stream selection: A behavioral and neural perspective," *Brain and Language*, vol. 122, no. 3, pp. 151–161, 2012.

[6] S. Gordon-Salant and P. J. Fitzgibbons, "Temporal factors and speech recognition performance in young and elderly listeners," *Journal of Speech and Hearing Research*, vol. 36, no. 6, pp. 1276–1285, 1993.

[7] D. R. Frisina and R. D. Frisina, "Speech recognition in noise and presbycusis: Relations to possible neural mechanisms," *Hearing Research*, vol. 106, no. 1-2, pp. 95–104, 1997.

[8] A. Wingfield, L. W. Poon, L. Lombardi, and D. Low, "Speed of processing in normal aging: Effects of speech rate, linguistic structure, and processing time," *Journal of Gerontology*, vol. 40, no. 5, pp. 579–585, 1985.

[9] P. Mick, I. Kawachi, and F. R. Lin, "The association between hearing loss and social isolation in older adults," *Otolaryngology–Head and Neck Surgery*, vol. 150, no. 3, pp. 378–384, 2014.

[10] E. M. Chia, J. J. Wang, E. Rochtchina, R. R. Cumming, P. Newall, and P. Mitchell, "Hearing impairment and health-related quality of life: The blue mountains hearing study," *Ear and Hearing*, vol. 28, no. 2, pp. 187–195, 2007.

[11] K. G. Herbst and C. Humphrey, "Hearing impairment and mental state in the elderly living at home," *British Medical Journal*, vol. 281, no. 6245, pp. 903–905, 1980.

[12] F. R. Lin, L. Ferrucci, Y. An, J. O. Goh, J. Doshi, E. J. Metter, C. Davatzikos, M. A. Kraut, and S. M. Resnick, "Association of hearing impairment with brain volume changes in older adults," *NeuroImage*, vol. 90, pp. 84–92, 2014.

[13] G. A. Gates, M. L. Anderson, S. M. McCurry, M. P. Feeney, and E. B. Larson, "Central auditory dysfunction as a harbinger of Alzheimer dementia," *Archives of Otolaryngology–Head & Neck Surgery*, vol. 137, no. 4, pp. 390–395, 2011.

[14] E. R. Kandel, J. H. Schwartz, T. M. Jessell, S. A. Siegelbaum, and A. J. Hudspeth, *Principles of Neural Science*. New York: McGraw-Hill, 2013.

[15] G. Ehret and R. Romand, *The Central Auditory System*. Oxford: Oxford University Press, 1996.

[16] B. R. Schofield, S. D. Motts, J. G. Mellott, and N. L. Foster, "Projections from the dorsal and ventral cochlear nuclei to the medial geniculate body," *Frontiers in Neuroanatomy*, vol. 8, no. 10, 2014.

[17] J. B. Kelly and D. M. Caspary, "Chapter 9: Pharmacology of the inferior colliculus," in *The Inferior Colliculus* (J. A. Winer and C. Schreiner, eds.), pp. 248–281, New York: Springer, 2005.

[18] B. J. Slater, A. M. Willis, and D. A. Llano, "Evidence for layer-specific differences in corticocollicular neurons," *Neuroscience*, vol. 229, pp. 144–154, 2013.

[19] W. C. Loftus, D. C. Bishop, and D. L. Oliver, "Differential patterns of inputs create functional zones in central nucleus of inferior colliculus," *The Journal of Neuroscience*, vol. 30, no. 40, pp. 13396–13408, 2010.

[20] T. Ito and D. L. Oliver, "The basic circuit of the IC: Tectothalamic neurons with different patterns of synaptic organization send different messages to the thalamus," *Frontiers in Neural Circuits*, vol. 6, no. 48, 2012.

[21] D. H. Hubel and T. N. Wiesel, "Receptive fields of single neurones in the cat's striate cortex," *Journal of Physiology*, vol. 148, pp. 574–591, 1959.

[22] H. B. Barlow, "Summation and inhibition in the frog retina," *Journal of Physiology*, vol. 119, pp. 69–88, 1953.

[23] D. H. Hubel and T. N. Wiesel, "Receptive fields, binocular interaction and functional architecture in the cat's visual cortex," *Journal of Physiology*, vol. 160, pp. 106–154, 1962.

[24] A. R. Palmer, T. M. Shackleton, C. J. Sumner, O. Zobay, and A. Rees, "Classification of frequency response areas in the inferior colliculus reveals continua not discrete classes," *Journal of Physiology*, vol. 591, no. 16, pp. 4003–4025, 2013.

[25] L. M. Miller, M. A. Escabi, H. L. Read, and C. E. Schreiner, "Functional convergence of response properties in the auditory thalamocortical system," *Neuron*, vol. 32, no. 1, pp. 151–160, 2001.

[26] F. E. Theunissen, K. Sen, and A. J. Doupe, "Spectral-temporal receptive fields of nonlinear auditory neurons obtained using natural sounds," *The Journal of Neuroscience*, vol. 20, no. 6, pp. 2315–2331, 2000.

[27] C. Chen, F. C. Rodriquez, H. L. Read, and M. A. Escabi, "Spectrotemporal sound preferences of neighboring inferior colliculus neurons: Implication for local circuitry and processing," *Frontiers in Neural Circuits*, vol. 6, no. 62, 2012.

[28] C. A. Atencio, T. O. Sharpee, and C. E. Schreiner, "Receptive field dimensionality increases from the auditory midbrain to cortex," *Journal of Neurophysiology*, vol. 107, no. 10, pp. 2594–2603, 2012.

[29] S. Andoni and G. D. Pollak, "Selectivity for spectral motion as a neural computation for encoding natural communication signals in bat inferior colliculus," *Journal of Neuroscience*, vol. 31, no. 46, pp. 16529–16540, 2011.

[30] L. Wang, S. Devore, B. Delgutte, and H. S. Colburn, "Dual sensitivity of inferior colliculus neurons to itd in the envelopes of high-frequency sounds: Experimental and modeling study," *Journal of Neurophysiology*, vol. 111, pp. 164–181, 2014.

[31] M. Ono and D. L. Oliver, "The balance of excitatory and inhibitory synaptic inputs for coding sound localization," *Journal of Neuroscience*, vol. 34, no. 10, pp. 3779–3792, 2014.

[32] C. F. B. Murphy and E. Schochat, "How auditory temporal processing deficits relate to dyslexia," *Brazilian Journal of Medical and Biological Research*, vol. 42, no. 7, pp. 647–654, 2009.

[33] G. Musacchia, M. Sams, E. Skoe, and N. Krause, "Musicians have enhanced subcortical auditory and audiovisual processing of speech and music," *Proceedings of the National Academy of Sciences U.S.A*, vol. 104, no. 40, pp. 15894–15898, 2007.

[34] A. Parthasarathy and E. L. Bartlett, "Age-related auditory deficits in temporal processing in f-344 rats," *Neuroscience*, vol. 192, pp. 619–630, 2011.

[35] A. Parthasarathy and E. L. Bartlett, "Two-channel recording of auditory-evoked potentials to detect age-related deficits in temporal processing," *Hearing Research*, vol. 289, no. 1-2, pp. 52–62, 2012.

[36] U. C. Leong, K. Barsz, P. D. Allen, and J. P. Walton, "Neural correlates of age-related declines in frequency selectivity in the auditory midbrain," *Neurobiology of Aging*, vol. 32, pp. 168–178, 2011.

[37] P. S. Palombi and D. M. Caspary, "Physiology of the aged fischer 344 rat inferior colliculus: Responses to contralateral monaural stimuli," *Journal of Neurophysiology*, vol. 76, no. 5, pp. 3114–3125, 1996.

[38] D. M. Caspary, T. M. Holder, L. F. Hughes, J. C. Milbrandt, R. M. McKernan, and D. K. Naritoku, "Age-related changes in gabaa receptor subunit composition and function in rat auditory system," *Neuroscience*, vol. 93, no. 1, pp. 307–312, 1999.

[39] J. R. Engle, D. T. Gray, H. Turner, J. B. Udell, and G. H. Recanzone, "Age-related neurochemical changes in the rhesus macaque inferior colliculus," *Frontiers in Aging Neuroscience*, vol. 6, no. 73, 2014.

[40] L. Khouri, N. A. Lesica, and B. Grothe, "Impaired auditory temporal selectivity in the inferior colliculus of aged mongolian gerbals," *The Journal of Neuroscience*, vol. 31, no. 27, pp. 9958–9970, 2011.

[41] A. L. Hodgkin and A. F. Huxley, "A quantitative description of membrane current and its application to conduction and excitation in nerve," *Journal of Physiology*, vol. 117, pp. 500–544, 1952.

[42] J. B. Hagen, "The origins of bioinformatics," *Nature Reviews. Genetics*, vol. 1, pp. 231–236, 2000.

[43] M. Barinaga, "Neuroscience models the brain," *Science*, vol. 247, pp. 524–526, 1990.

[44] X. Zhang, M. G. Heinz, I. C. Bruce, and L. H. Carney, "A phenomenological model for the responses of auditory nerve fibers: I. nonlinear tuning with compression and surpression.," *Journal of the Acoustical Society of America*, vol. 109, no. 2, pp. 648–670, 2001.

[45] I. C. Bruce, M. B. Sachs, and E. D. Young, "An auditory-periphery model of the effects of acoustic trauma on auditory nerve responses," *Journal of the Acoustical Society of America*, vol. 113, no. 1, pp. 369–388, 2003.

[46] M. S. A. Zilany and I. C. Bruce, "Modeling auditory-nerve responses for high sound pressure levels in the normal and impaired auditory periphery," *Journal of the Acoustical Society of America*, vol. 120, no. 3, pp. 1446–1466, 2006.

[47] A. Chintanpalli, S. G. Jennings, M. G. Heinz, and E. A. Strickland, "Modeling the anti-masking effects of the olivocochlear reflex in auditory nerve responses to tones in sustained noise," *Journal of the Association for Research in Otolaryngology*, vol. 13, pp. 219–235, 2012.

[48] J. Swaminathan and M. G. Heinz, "Psychophysiological analyses demonstrate the importance of neural envelope coding for speech perception in noise," *Journal of Neuroscience*, vol. 32, no. 5, pp. 1747–1756, 2012.

[49] O. Lomakin and K. A. Davis, "On the role of the wideband inhibitor in the dorsal cochlear nucleus: A computational modeling study," *Journal of the Association of Research in Otolaryngology*, vol. 9, pp. 506–520, 2008.

[50] M. J. Spencer, D. B. Grayden, I. C. Bruce, H. Meffin, and A. N. Burkitt, "An investigation of dendritic delay in octopus cells of the mammalian cochlear nucleus," *Frontiers of Computational Neuroscience*, vol. 6, no. 83, 2012.

[51] Z. Bures and P. Marsalek, "On the precision of neural computation with iteraural level differences in the lateral superior olive," *Brain Research*, vol. 1536, pp. 16–26, 2013.

[52] M. J. Fischl, T. D. Combs, A. Klug, B. Grothe, and R. M. Burger, "Modulation of synaptic input by gabab receptors imporves coincidence detection for computation of sound location," *Journal of Physiology*, vol. 590, no. Pt. 13, pp. 3047–3066, 2012.

[53] C. F. Rabang, A. Parthasarathy, Y. Venkataraman, Z. L. Fisher, S. M. Gardner, and E. L. Bartlett, "A computational model of inferior colliculus responses to amplitude modulated sounds in young and aged rats," *Frontiers In Neural Circuits*, vol. 6, no. 77, 2012.

[54] P. C. Nelson and L. H. Carney, "A phenomenological model of peripheral and central neural responses to amplitude-modulated tones," *Journal of the Acoustical Society of America*, vol. 116, no. 4 pt. 1, pp. 2173–2186, 2004.

[55] C. F. Rabang and E. L. Bartlett, "A computational model of cellular mechanisms of temporal coding in the medial geniculate body (MGB)," *PLoS One*, vol. 6, no. 12, 2011.

[56] M. de Pinho, M. Mazza, and A. C. Roque, "A computational model of primary auditory cortex exhibiting plasticity in the frequency representation," *Neurocomputing*, vol. 70, pp. 3–8, 2006.

[57] A. A. Prinz, L. F. Abbott, and E. Marder, "The dynamic clamp comes of age," *TRENDs in Neuroscience*, vol. 27, no. 4, pp. 218–224, 2004.

[58] N. T. Carnevale and M. L. Hines, *The NEURON Book*. Cambridge, UK: Cambridge University Press, 2006.

[59] D. M. Caspary, T. A. Schatteman, and L. F. Hughes, "Age-related changes in the response properties of cartwheel cells in rat dorsal cochlear nucleus," *Hearing Research*, vol. 216-217, pp. 207–215, 2006.

[60] A. G. Paolini, E. L. Cotterill, D. Bairaktaris, and G. M. Clark, "Muscimol suppression of the dorsal cochlear nucleus modifies frequency tuning in rats," *Brain Research*, vol. 785, no. 2, pp. 309–316, 1998.

[61] U. Ebert and J. Ostwald, "Gaba alters the discharge patterns in the rat ventral cochlear nucleus," *Hearing Research*, vol. 91, no. 1-2, pp. 160–166, 1995.

[62] N. K. Woolf and A. F. Ryan, "Ontogeny of neural discharge patterns in the ventral cochlear nucleus of the mongolian gerbil," *Brain Research*, vol. 349, no. 1–2, pp. 131–147, 1985.

[63] N. Greene, O. Lomakin, and K. Davis, "Monoaural spectral processing differs between lateral superior olive and inferior colliculus: Physiological evidence for an acoustic chiasm," *Hearing Research*, vol. 269, no. 1-2, pp. 134–145, 2010.

[64] P. G. Finlayson and D. M. Caspary, "Response properties in young and old fischer-344 rat lateral superior olive neurons: A quantitative approach," *Neurobiology of Aging*, vol. 14, pp. 127–139, 1993.

[65] J. B. Kelly, A. D. Buckthought, and S. A. Kidd, "Monoaural and binaural properties of single neurons in the rat's dorsal nucleus of the lateral lemniscus," *Hearing Research*, vol. 122, no. 1-2, pp. 25–40, 1998.

[66] H. Zhang and J. B. Kelly, "Response of neurons in the rat's ventral nucleus of the lateral lemniscus to monoaural and binaural tone bursts," *Journal of Neurophysiology*, vol. 95, no. 4, pp. 2501–2512, 2006.

[67] L. Devroye, *Non-Uniform Random Variate Generation*. New York: Springer-Verlag, 1986.

[68] J. A. Garcia-Lazaro, L. A. Belliveau, and N. A. Lesica, "Independent population coding of speech with sub-millisecond precision," *Journal of Neuroscience*, vol. 33, no. 49, pp. 19362–19372, 2013.

[69] A. G. Paolini and G. M. Clark, "Intracellular responses of onset chopper neurons in the ventral cochlear nucleus to tones: Evidence for dual-component processing," *Journal of Neurophysiology*, vol. 81, pp. 2347–2359, 1999.

[70] M. Rudolph and A. Destexhe, "Inferring network activity from synaptic noise," *Journal of Physiology-Paris*, vol. 98, no. 4-6, pp. 452–466, 2004.

[71] A. Destexhe, M. Rudolph, J. M. Fellous, and T. J. Sejnowski, "Fluctuating synaptic conductances recreate in-vivo-like activity in neocortical neurons," *Neuroscience*, vol. 107, pp. 13–24, 2001.

[72] J. Kennedy and R. Eberhart, "Particle swarm optimization," in *Neural Networks, 1995. Proceedings., IEEE International Conference on*, vol. 4, pp. 1942–1948 vol.4, Nov 1995.

[73] U. Jaimini and V. K. Panchal, "Swarm intelligence computational paradigm," in *Emerging Trends in Communication, Control, Signal Processing Computing Applications (C2SPCA), 2013 International Conference on*, pp. 1–8, Oct 2013.

[74] R. Poli, J. Kennedy, and T. Blackwell, "Particle swarm optimization: An overview," *Swarm Intelligence*, vol. 1, pp. 33–57, 2007.

[75] R. Mendes, J. Kennedy, and J. Neves, "The fully informed particle swarm: Simpler, maybe better," *IEEE Transactions on Evolutionary Computation*, vol. 8, no. 3, pp. 204–210, 2004.

[76] I. Lampl, D. Ferster, T. Poggio, and M. Riesenhuber, "Intracellular measurements of spatial integration and the max operation in complex cells of the cat primary visual cortex," *Journal of Neurophysiology*, vol. 92, pp. 2704–2713, 2004.

[77] A. Oleksiak, P. C. Klink, A. Postma, I. J. van der Ham, M. J. Lankheet, and R. J. A. van Wezel, "Spatial summation in macaque parietal area 7a follows a winner-take-all rule," *Journal of Neurophysiology*, vol. 105, pp. 1150–1158, 2011.

[78] H. H. Rosenbrock, "An automatic method for finding the greatest or least value of a function," *The Computer Journal*, vol. 3, no. 3, pp. 175–184, 1960.

[79] Y.-W. Shang and Y.-H. Qiu, "A note on the extended rosenbrock function," *Evolutionary Computation*, vol. 14, no. 1, pp. 119–126, 2006.

[80] D. H. Wolpert and W. G. Macready, "No free lunch theorems for optimization," *IEEE Transactions on Evolutionary Computation*, vol. 1, no. 1, pp. 67–82, 1997.

[81] G. Y. Zhu and W. B. Zhang, "Drilling path optimization by the particle swarm optimization algorithm with global convergence characteristics," *International Journal of Production Research*, vol. 46, no. 8, pp. 2299–2311, 2008.

[82] J. Tiilikainen, V. Bosund, M. Mattila, T. Hakkarainen, J. Sormunen, and H. Lipsanen, "Fitness function and nonunique solutions in x-ray reflectivity curve fitting: Crosserror between surface roughness and mass density," *Journal of Physics D: Applied Physics*, no. 40, pp. 4259–4263, 2007.

[83] M. Afshar, "Large scale reservoir operation by constrained particle swarm optimization algorithms," *Journal of Hydro-environment Research*, vol. 6, no. 1, pp. 75–87, 2012.

[84] C. A. C. Coello, "Theoretical and numerical constraint-handling techniques used with evolutionary algorithms: A survey of the state of the art," *Computer Methods in Applied Mechanics and Engineering*, vol. 191, no. 11–12, pp. 1245–1287, 2002.

[85] M. Bastian, S. Heymann, and M. Jacomy, "Gephi: An open source software for exploring and manipulating networks," in *International AAAI Conference on Weblogs and Social Media*, pp. 1–2, 2009.

APPENDICES

A. MODEL VALUES AND PARAMETERS

The following tables are model neuron parameter values. These have been adapted from [53]. Figure A.1 gives a basic block diagram of the model.
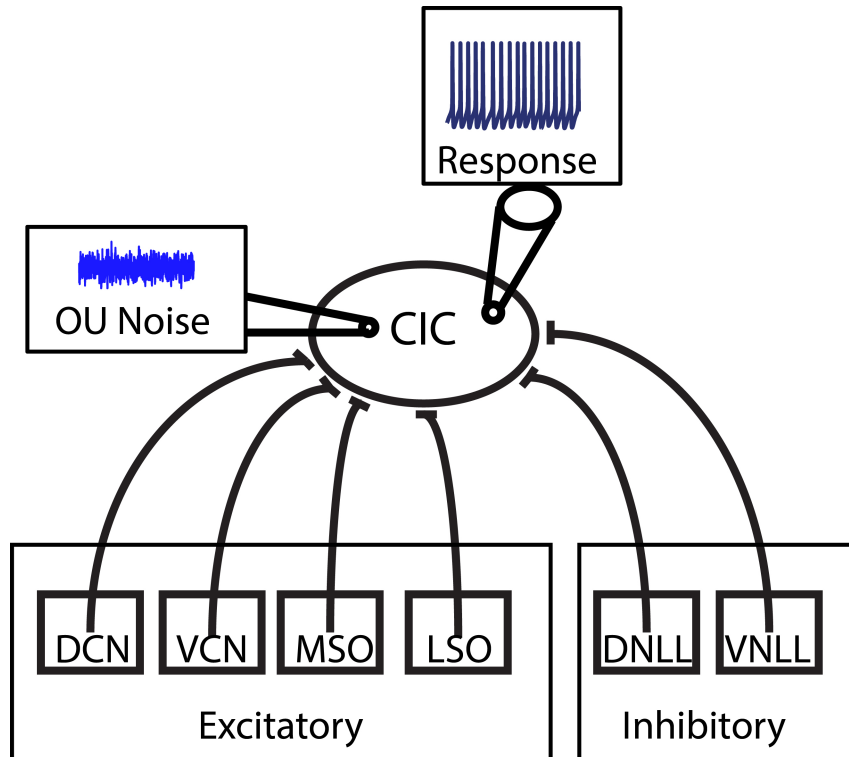

Fig. A.1. Block Diagram of the IC Neuron Model. The Model Receives Excitatory projections from DCN,VCN,MSO, and LSO and inhibitory projections from DNLL and VNLL. A point process noise current in injected into the center of the model cell.

Table A.1: Sustained Firing Model

Parameter	Value
Cell Body Diameter	32.65 um
Cell Body Length	32.65 um
Axial Resistance	150 ohm-cm
Passive Mean Conductance	.19 mS
Passive Reversal Potential	-70 mV
Fast Transient Sodium Mean Conductance	.1 mS
Fast Transient Sodium Reversal Potential	50 mV
Delayed Rectifier Potassium Mean Conductance	.1 mS
Delayed Rectifier Reversal Potential	-90 mV
High Threshold Potassium Mean Conductance	0.005 mS
High Threshold Potassium Reversal Potential	-90
TEA sensitive Potassium Mean Conductance	0.014 mS
TEA sensitive Potassium Reversal Potential	-90 mV
Low Threshold Potassium Mean Conductance	0 mS
Low Threshold Potassium Reversal Potential	-90 mV

Table A.2: Adapting Model

Parameter	Value
Cell Body Diameter	34.5 um
Cell Body Length	34.5 um
Axial Resistance	150 ohm-cm
Passive Mean Conductance	.149 mS
Passive Reversal Potential	-70 mV
Fast Transient Sodium Mean Conductance	.2 mS
Fast Transient Sodium Reversal Potential	50 mV
TEA sensitive Potassium Mean Conductance	0 mS
TEA sensitive Potassium Reversal Potential	-85 mV
Low Threshold Potassium Mean Conductance	0 mS
Low Threshold Potassium Reversal Potential	-90 mV

Table A.3: O-U Noise Conductance Parameters

Parameter	Value
Mean Excitatory Conductance	.935 nS
Mean Inhibitory Conductance	.5 nS
Excitatory Conductance Standard Deviation	.8891 nS
Inhibitory Conductance Standard Deviation	.5 nS
Excitatory Conductance Time Constant	2 ms
Inhibitory Conductance Time Constant	10 ms
Mean Firing Rate	2.236 Spks/s
Firing rate Standard Deviation	.6162

B. PARTICLE SWARM PARAMETERS

B.1 WTA PSO parameters

The following Table describes relevant parameters for the proposes PSO social network. All graph analysis was performed using Gephi [85]. Average path length is a metric which quantifies the shortest path distance from one arbitrary node in the graph to another. The diameter of a graph describes the greatest distance from a given node to another node. The radius is a global network measure which, looks for the minimum max distance between two nodes. Modularity quantifies the graph's division into smaller subset components. Finally, the average clustering component describes how nodes are connected in neighborhoods.

Table B.1: Swarm Social Network Parameters

Parameter	Value
Avg. Path Length	2.971
Diameter	4
Radius	2
Modularity	.664
Avg. Clustering Coeff	.584

B.2 Ring Topology

The ring topology is a common network used in PSO [75]. Our implementation only polled data from surrounding neighbors for update. Unless an agent is connected

to the global leader, no direct influence is created. Topology can be seen in Figure B.1. Graph metrics for the Ring topology are found in Table B.1
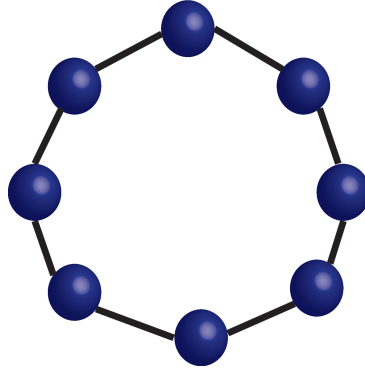
Ring Topology

Fig. B.1. Network diagram of the ring network

Table B.2: Swarm Social Network Parameters

Parameter	Value
Avg. Path Length	5.5
Diameter	10
Radius	10
Modularity	.56
Avg. Clustering Coeff	0

The ring network was updated as follows:

$$v_{i+1} = \chi * (v_i + U(0, \phi 1) \otimes (p_l - x_i) + U(0, \phi 2) \otimes (p_r - x_i)) \tag{B.1}$$

$$x_{i+1} = x_i + v_{i+1} \tag{B.2}$$

where U is a random variable between 0 and $\phi_{1,2}$, $\phi_{1,2}$, χ are constriction variables, x_i is the current position of the variable being updated, $p_{l,r}$ correspond to the best position of the left and right updating agent respectively.

VITA

VITA

Brandon was born on August 13th, 1987 in Decatur Illinois. He received a Bachelor of Science in Electrical Engineering from Saint Louis University in 2012. His senior design project, "'Movement Assistance Technology and Engineering Parkinson's Assistance Device"' was awarded an ASEE/NISH development award and went on to win the award for outstanding senior design project in computer engineering. While at SLU, Brandon conducted research in cardiac signal processing and nonlinear biological systems under Cecil W. Thomas, PhD.

Brandon entered the department of electrical and computer engineering at Purdue University in the Fall of 2012. During his masters, Brandon worked in the Central Auditory Processing lab under the direction of Edward Bartlett, PhD. Brandon's research interests fall in the area of computational neuroscience, biomedical signal processing, and cochlear implant stimulation paradigms. Since coming to Purdue, Brandon has been inducted into Eta Kappa Nu, the electrical and computer engineering honors society.

In Fall 2014, Brandon will begin his PhD in Biomedical Engineering under a Ross Fellowship. He will continue his work under Edward Bartlett in the area of computational and systems neuroscience. In his down time, Brandon plays guitar or bass in several bands. He has three commercially available cds to his name.